# Preventing trogocytosis by cathepsin B inhibition augments CAR T cell function

Kenneth A. Dietze[1], Kiet Nguyen[2], Aashli Pathni[3], Frank Fazekas[2], Wenxiang Sun[4], Ethan Rosati[4], Jillian M. Baker[1], Maday Galeana Figueroa[5], Etse Gebru[6], Daniel Yamoah[6], Rediet Mulatu[6], Alexander Wang[1], Aaron P. Rapoport[6], David Lum[4], Xiaoxuan Fan[6], Sabarinath V. Radhakrishnan[5], Djordje Atanackovic[6], Arpita Upadhyaya[2,7,8], Tim Luetkens[1,6]

[1] Department of Microbiology and Immunology, University of Maryland School of Medicine, Baltimore, MD, USA

[2] Biophysics Graduate Program, University of Maryland, College Park, MD, USA

[3] Biological Sciences Graduate Program, University of Maryland, College Park, MD, USA

[4] Preclinical Research Resource, Huntsman Cancer Institute, Salt Lake City, UT, USA

[5] Division of Hematology and Oncology, Medical College of Wisconsin, Milwaukee, WI, USA

[6] Department of Medicine and Transplant/Cell Therapy Program, University of Maryland School of Medicine and Marlene and Stewart Greenebaum

[7] Institute for Physical Science and Technology, University of Maryland, College Park, MD, USA

[8] Department of Physics, University of Maryland, College Park, MD, USA

One sentence summary: CAR-mediated trogocytosis is mediated by the cysteine protease cathepsin B and directly causes CAR T cell exhaustion and fratricide.

Word count (abstract): 237

Word count (main text): 7,227

Figures/Tables: 6 Figures, 7 Suppl. Figures, 1 Suppl. Table

*Corresponding author:
Tim Luetkens, M.D.
Associate Professor of Microbiology and Immunology
Director R&D at Fannie Angelos Cellular Therapeutics Laboratory
University of Maryland
655 W Baltimore St, RM. 9-009
Baltimore, MD 21201
Phone: 410-706-1924
Email: tluetkens@som.umaryland.edu

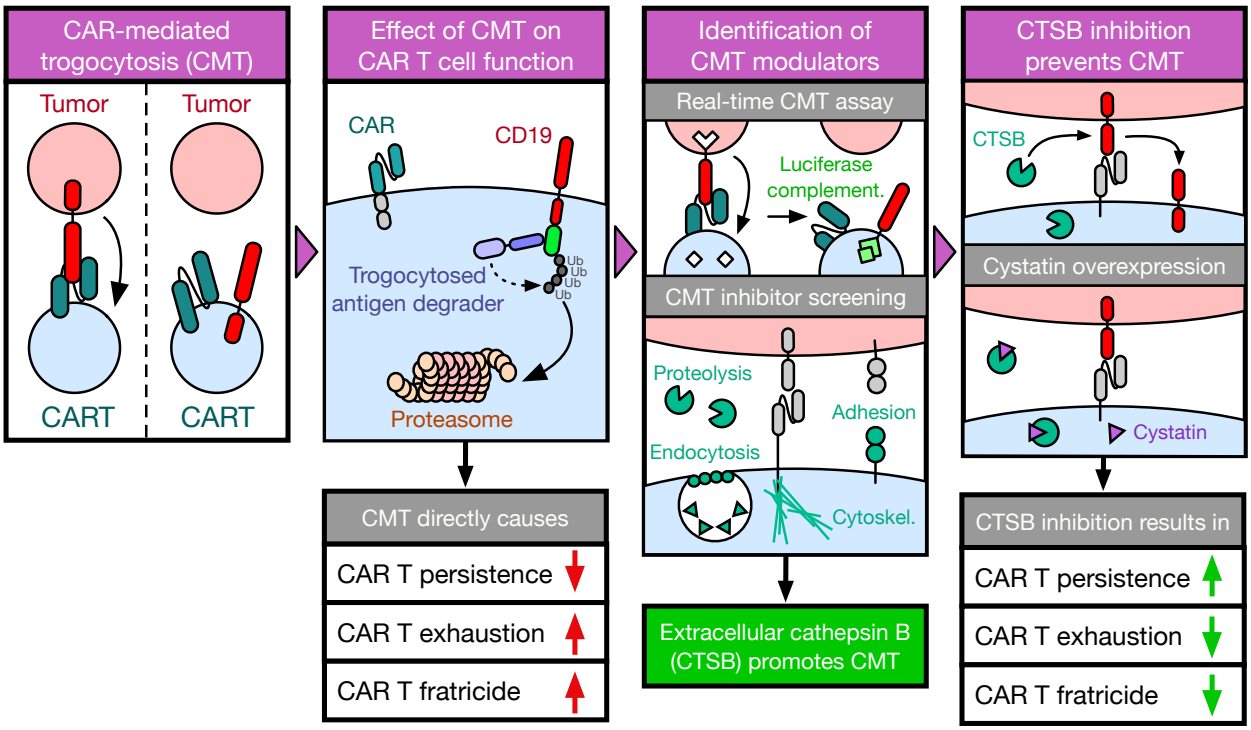


## ABSTRACT

Chimeric antigen receptor (CAR) T cell therapy has shown remarkable efficacy in cancer treatment. Still, most patients receiving CAR T cells relapse within 5 years of treatment. CAR-mediated trogocytosis (CMT) is a potential tumor escape mechanism in which cell surface proteins transfer from tumor cells to CAR T cells. CMT results in the emergence of antigen-negative tumor cells, which can evade future CAR detection, and antigen-positive CAR T cells, which has been suggested to cause CAR T cell fratricide and exhaustion. Whether CMT indeed causes CAR T cell dysfunction and the molecular mechanisms conferring CMT remain unknown. Using a selective degrader of trogocytosed antigen in CAR T cells, we show that the presence of trogocytosed antigen on the CAR T cell surface directly causes CAR T cell fratricide and exhaustion. By performing a small molecule screening using a custom high throughput CMT-screening

46 assay, we found that the cysteine protease cathepsin B is essential for CMT and that
47 inhibition of cathepsin B is sufficient to prevent CAR T cell fratricide and exhaustion,
48 leading to improved long-term CAR T cell persistence and anti-tumor activity. Our data
49 demonstrate that it is feasible to separate CMT from cytotoxic activity, that CAR T cell
50 persistence, a key factor associated with clinical CAR T cell efficacy, is directly linked to
51 cathepsin B activity in CAR T cells, and that it is possible to improve CAR T cell function
52 through selective inhibition of CMT.

53 **INTRODUCTION**

54 Chimeric antigen receptors (CAR) are genetically engineered proteins combining antigen
55 binding domains with immune cell activation domains[1–3]. T cells and natural killer (NK)
56 cells can be engineered to express CARs to recognize tumor-associated antigens with
57 high specificity and have been shown to be clinically effective at targeting several
58 hematological malignancies[1,4–7]. Currently, seven CAR T cell approaches targeting CD19
59 or B cell maturation antigen (BCMA) have been approved in the US for the treatment of
60 hematological cancers[8,9]. While CAR T cell therapy has greatly improved clinical
61 outcomes for patients, many patients still relapse within five years of treatment[10–15].
62 Several factors have been implicated in CAR T cell-associated relapse, including
63 increased CAR T cell exhaustion[16], reduced CAR T cell expansion[17] and persistence[18,19],
64 as well as tumor antigen escape[18,2018,21].

65 It has previously been shown that CAR T cells and CAR NK cells rapidly transfer the
66 targeted antigen from tumor cells to their own cell surface in a process called
67 trogocytosis[22–24]. Trogocytosis was initially observed at the immune synapse between
68 conventional T cells and antigen presenting cells (APCs), where TCR internalization
69 following activation resulted in the transfer of MHC to recipient T cells[25,26]. CAR-mediated
70 trogocytosis (CMT) occurs in both hematological and solid tumors and is correlated with
71 increased expression of apoptotic and exhaustion markers on CAR T cells, as well as
72 reduced persistence and expansion[22–24]. In addition, it has been shown that T cells
73 engineered to express the tumor antigen CD19 are efficiently killed by other CD19 CAR
74 T cells (“fratricide”)[22]. CMT is also implicated in a reduction of target antigen on the tumor

75 cell surface, leading to antigen-negative or antigen-low variants which could escape CAR
76 T cell detection[23]. Reductions in CAR T cell affinity have previously been shown to reduce
77 CMT[23], but this could lead to an increased antigen threshold[27], preventing the detection
78 of antigen-low tumor cells.

79 Mechanistically linking CMT to exhaustion, fratricide, and reduced CAR T cell persistence
80 has, so far, been elusive due to the lack of specific inhibitors of trogocytosis. In this study,
81 we develop an analytical framework to investigate CMT and determine the effects of CMT
82 on CAR T cell function as well as its mechanistic basis. In addition, we demonstrate how
83 CMT can be specifically targeted by inhibiting the protease cathepsin B using
84 endogenous inhibitors to increase CAR T cell persistence and enhance long-term anti-
85 tumor activity.

86 **RESULTS**

87 *CAR T cells acquire target antigen via trogocytosis*

88 CAR-mediated trogocytosis (CMT) is the extraction of the targeted tumor antigen from
89 the tumor cell surface and its incorporation into the CAR T cell plasma membrane[22–24,28]
90 (Suppl. Fig. S1A). *Ex vivo*, CMT occurs across cancer types[22,23] and target antigens,
91 including CD19[22–24], CD22[22], mesothelin[22], and BCMA[28]. We found robust transfer of
92 CD19 to CD19-targeting CAR T cells (clone: FMC63, Suppl. Fig. S1B) as well as CD19
93 loss on tumor cells (Suppl. Fig. S1C), which can be observed minutes after CAR T cells
94 contact target cells (Fig. 1A, Suppl Fig. S1D). Similarly, we confirmed transfer of *B cell*
95 *maturation antigen* (BCMA), the target of two clinically approved CAR T cell approaches
96 for the treatment of multiple myeloma[4,5,29,30] (Fig. 1B) to BCMA CAR T cells (Fig. 1C) and
97 loss of BCMA from tumor cells (Fig. 1D) independent of BCMA binding domain (Fig. 1B).
98 When assessing CMT in solid tumor models *in vitro*, we observed significant transfer of
99 target antigen to CAR T cells targeting LINGO1 (Suppl. Fig. S1E), GD2 (Suppl. Fig. S1F),
100 and FolRα (Suppl. Fig. S1G). In the clinical setting, CMT has only been shown to occur
101 in B cell lymphoma patients treated with CAR NK cells[24]. By analyzing peripheral blood
102 mononuclear cells (PBMCs) from patients who had recently received CD19 CAR T cells,
103 we demonstrate that CMT also occurs in some patients treated with CAR-expressing T
104 cells (Fig. 1E/F, Suppl. Fig. S1H). Further analyzing a sample from a patient with a high
105 number of $CD19^{+}$ CAR T cells, we found that the presence of CD19 on CAR T cells was
106 associated with increased amounts of the exhaustion markers PD-1 and TIM-3 (Suppl.
107 Fig. S1I).

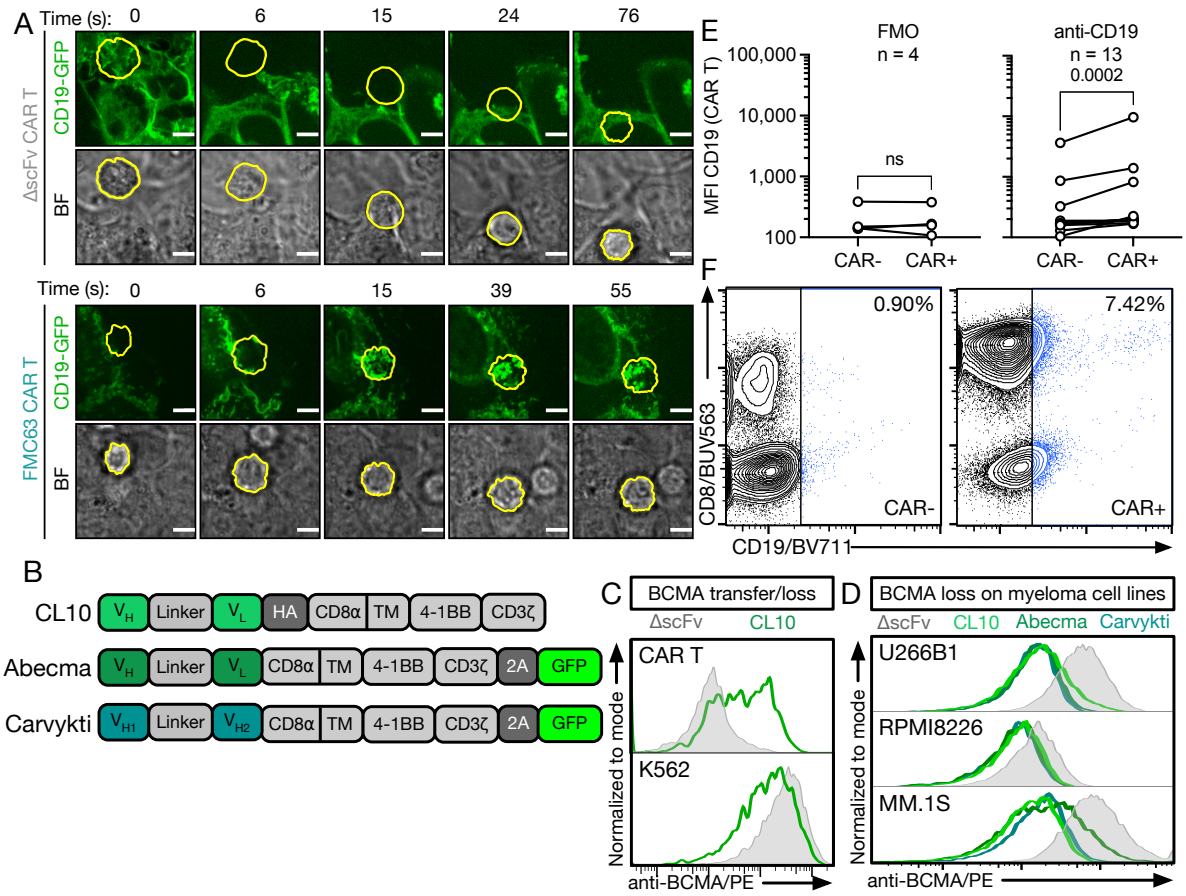


**Figure 1: CD19 and BCMA CAR T cells rapidly acquire target antigen via trogocytosis. (A)** Observation of CMT in brightfield (BF) and confocal images of ΔscFv or FMC63 CAR T cells. CAR T cells were cultured with plate-bound 293T cells expressing a CD19-GFP fusion protein. CD19 is shown in green. Individual CAR T cells are circled in yellow and tracked over time. Scale bar represents 5$\mu$m. Data is representative of cells from two independent experiments. **(B)** Schema of BCMA-targeting CAR T cell products. The same PBMC donor was used to produce Abecma and Carvykti CAR T cells; due to availability, a separate donor was used to produce CL10 CAR T cells. **(C)** BCMA transfer to CAR T cells (top) and BCMA loss on BCMA-GFP-expressing K562 cells (bottom) as determined by flow cytometry. **(D)** BCMA loss on MM.1S, RPMI8226, and U266B1 cells when cocultured with CL10[31] , Abecma, and Carvykti CAR T cells as determined by flow cytometry. **(C/D)** Data is representative of three independent experiments. **(E)** Amount of CD19 on CAR T cells (CAR$^+$) or non-CAR T cells (CAR$^-$) in PBMCs isolated

121 from patients 7-28 days after receiving CD19 CAR T cell therapy using full-spectrum flow cytometry. Data
122 indicate values from individual patient samples (FMO n = 4; anti-CD19 n = 13). Statistical significance was
123 determined by Wilcoxon matched-pairs signed-rank test. Fluorescence-minus-one (FMO) refers to staining
124 with full flow cytometry panel except anti-CD19. **(F)** Representative flow cytometry data from one patient
125 depicting CD19 levels on $CAR^-$ and $CAR^+$ T cells. CAR was stained using an anti-idiotype antibody.
126

127 *CAR-mediated trogocytosis directly causes CAR T cell dysfunction*

128 The presence of trogocytosed antigen on CAR T cells is correlated with increased
129 exhaustion and reduced viability[22–24] but it remains unknown if CMT directly causes this
130 T cell dysfunction. To answer this question, we developed an approach for the targeted
131 degradation of trogocytosed CD19 fused to GFP (CD19-GFP) in CAR T cells (Fig. 2A).
132 To validate the approach, we first expressed CD19-GFP as well as a trogocytosed
133 antigen degrader (TAD), the E3-targeting domain Nslmb[32,33] fused to a GFP-binding
134 protein ($TAD_{GFP}$), in 293T cells. TAD overexpression resulted in a significant reduction of
135 total CD19, with multiple CD19 bands likely reflecting differential glycosylation[34,35] (Suppl
136 Fig. S2A), and surface CD19-GFP (Suppl Fig. S2A/B). We next generated CAR T cells
137 expressing $TAD_{GFP}$ and did not observe an effect of $TAD_{GFP}$ on CAR T cell expansion or
138 short-term antitumor activity (Suppl Fig. S2C/D).

139 When cocultured for 2 hours with K562 cells expressing CD19-GFP, conventional FMC63
140 CAR T cells showed increased levels of CD19 (Fig. 2B, Suppl. Fig. S2E) and GFP (Fig.
141 2C, Suppl. Fig. S2F) indicative of CMT, as expected. However, FMC63 CAR T cells also
142 expressing $TAD_{GFP}$ showed an approximately 50% reduction in both CD19 and GFP after
143 coculture. Using the TAD system, we next investigated the effect of CMT on CAR T cell
144 fratricide. We found that $TAD_{GFP}$ expression did not alter the proliferation of CAR T cells
145 when co-cultured with $CD19^{+}$ tumor cells (Suppl. Fig. S2G). However, $TAD_{GFP}$ expression
146 resulted in a two-fold increase in CAR T cell numbers after co-culture (Fig. 2D), indicating
147 that CMT directly causes CAR T cell death, likely due to fratricide. Targeted degradation
148 of trogocytosed antigen was also validated using a fully human TAD ($TAD_{CD19}$) construct

149 directly targeting CD19. $TAD_{CD19}$ recognizes CD19 by using the Lyn kinase SH2 domain
150 (Fig. 2E), which has been shown to bind the intracellular domain of CD19 with high
151 affinity[36]. Co-expression of $TAD_{CD19}$ in FMC63 CAR T cells also resulted in reduced CMT
152 (Fig. 2F/G). The reduction in CD19-GFP on the CAR T cell surface by $TAD_{CD19}$ was more
153 pronounced when measuring GFP (Fig. 2F) than CD19 (Fig. 2G), which may be the result
154 of CD19 CAR molecules binding to the trogocytosed CD19 in cis blocking the anti-CD19
155 detection antibody and thereby leading to an underestimation of CD19 on the CAR T cell
156 surface. These data indicate that selective degradation of trogocytosed antigen is feasible
157 in CAR T cells and that this approach can be used to explore the effects of CMT on CAR
158 T cell function.

159 It has previously been shown that FMC63 binding to CD19 in *cis*[37] can cause persistent
160 CAR signaling followed by T cell exhaustion. We found that conventional FMC63 CAR T
161 cells that had acquired CD19 during co-culture with CD19-GFP-expressing K562 cells
162 showed a two-fold increased expression of exhaustion markers LAG-3 and TIM-3
163 compared to negative control T cells expressing a CAR without a binding domain (ΔscFv,
164 Fig. 2H/I, Suppl. Fig. S2H/I). Expression of $TAD_{GFP}$ prevented LAG-3/TIM-3 upregulation
165 on these cells, demonstrating that increased exhaustion marker expression is the direct
166 consequence of trogocytic antigen transfer to CAR T cells. CMT-induced fratricide and
167 exhaustion could substantially limit long-term CAR T cell anti-tumor activity. In a serial
168 coculture stress test of CAR T cell efficacy (Fig. 2J), we found that $TAD_{GFP}$ substantially
169 increased the ability of CAR T cells to control B cell acute lymphoblastic leukemia (B-ALL,
170 Fig. 2K).

171 These data demonstrate that CMT directly causes CAR T cell dysfunction and fratricide,

172 thereby limiting CAR T cell persistence and anti-tumor activity.

173

174

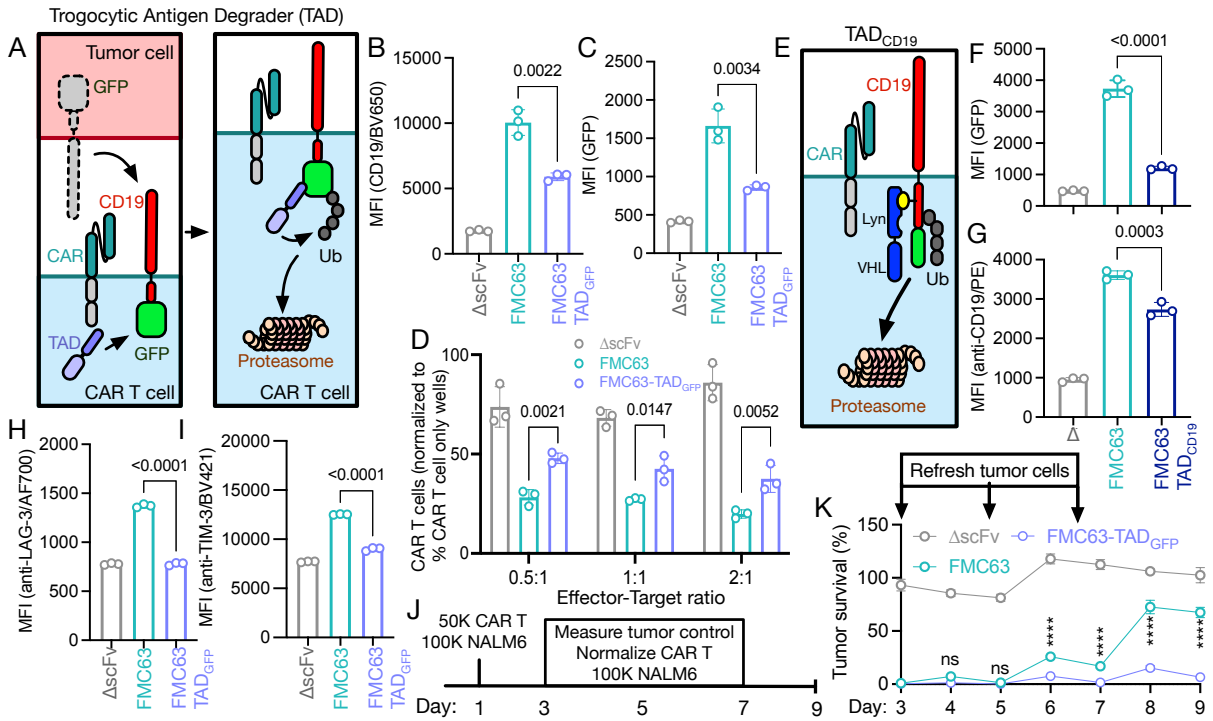


175

176 **Figure 2: CAR-mediated trogocytosis directly causes CAR T cell dysfunction. (A)** Schema of
177 trogocytosed antigen degrader (TAD). **(B)** CD19 and **(C)** GFP expression on FMC63 CAR T cells
178 expressing $TAD_{GFP}$ or T cells expressing a CAR lacking a binding domain (ΔscFv) following a 2-hour
179 coculture with CD19-GFP-expressing NALM6 cells as determined by flow cytometry. Data indicates mean
180 ± S.D. from three technical replicates. **(D)** Quantification of CAR T cells after a 24-hour coculture with CD19-
181 GFP-expressing NALM6 cells using flow cytometry. Values are normalized to wells containing only CAR T
182 cells. **(B-D)** Data indicates mean ± S.D. from three technical replicates. Data is representative of three
183 independent experiments. **(E)** Schema of a fully human-derived TAD system ($TAD_{CD19}$). Lyn = SH2 domain
184 of lyn kinase; VHL = von Hippel-Lindau protein; Ub = ubiquitin. **(F)** GFP and **(G)** CD19 expression on FMC63
185 CAR T cells expressing $TAD_{CD19}$ or ΔscFv CAR T cells after a 2-hour coculture with CD19-GFP-expressing
186 NALM6 cells at a 0.5:1 effector-target ratio. Data indicates mean ± S.D. from three technical replicates.
187 Data is representative of two independent experiments. **(H)** LAG-3 and **(I)** TIM-3 expression on CAR T cells
188 expressing $TAD_{GFP}$ as measured by MFI after a 24-hour coculture with CD19-GFP-expressing NALM6 cells
189 using full-spectrum flow cytometry. Data indicates mean ± S.D. from three technical replicates. Data is

190 representative of three independent experiments. **(B-D, F-I)** Statistical significance was determined by one-
191 way ANOVA. **(J)** Schema of *in vitro* serial coculture experiment to determine long-term CAR T cell
192 expansion and antitumor activity. CAR T cells were normalized and fresh tumor cells were added on days
193 3, 5, and 7. **(K)** Survival of CD19-GFP-expressing NALM6 cells expressing firefly luciferase (Fluc) at a 0.5:1
194 effector-target ratio using a luminescence-based cytotoxicity assay. Data indicates mean ± S.D. from three
195 technical replicates. Tumor survival was normalized to untreated tumor cells. Data is representative of two
196 independent experiments. Statistical significance comparing FMC63 and FMC63-$TAD_{GFP}$ was determined
197 by two-way ANOVA**.**

198 *Real-time detection of CAR-mediated trogocytosis by luciferase complementation assay*

199 Little is known regarding the molecular and cellular drivers of CMT, and to date there are
200 no high-throughput assays to systematically probe potential modulators of CMT as it
201 occurs in real-time. To address this, we developed a luciferase complementation assay
202 for the real-time detection of CMT (CompLuc, Fig. 3A). In the CompLuc assay, luciferase
203 complementation occurs following the transfer of CD19 fused to the C-terminal fragment
204 of NanoLuc[38] (cLuc) to CAR T cells, which express the complementary cytosolic N-
205 terminal NanoLuc (nLuc) fragment with high affinity for cLuc[38] (Fig. 3B, Suppl. Fig.
206 S3A/B). The CompLuc assay allows for sensitive detection of small numbers of
207 $nLuc^{+}cLuc^{+}$ CAR T cells in cocultures (Fig. 3C). We demonstrate that CMT, as quantified
208 by CompLuc, is antigen- and CAR-dependent, and correlates with effector-target ratio
209 (Fig. 3D-F) and antigen transfer as measured by flow cytometry (Fig. 3D/F).

210 To validate the CompLuc assay, we determined the effect of an established modulator of
211 CMT, the actin polymerization inhibitor cytochalasin D[22,39]. Treatment of CAR T cells with
212 cytochalasin D significantly reduced CMT in a dose-dependent manner as measured by
213 CompLuc (Fig. 3G), demonstrating the ability of the assay to identify modulators of CMT.
214

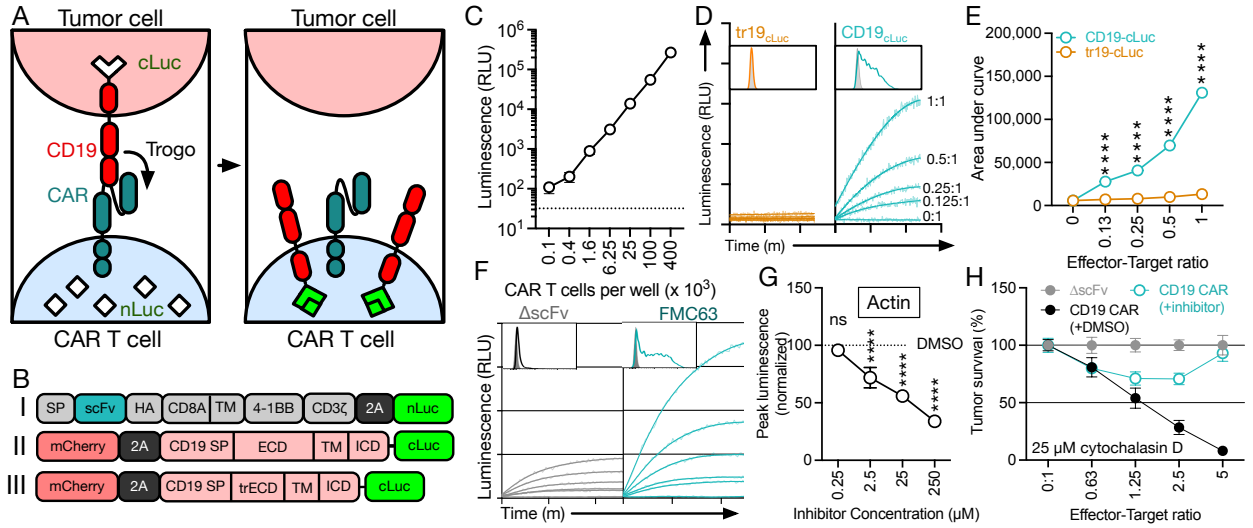


**Figure 3: Luciferase complementation assay allows for the real-time detection of trogocytosis. (A)** Schema of luciferase complementation assay (CompLuc). **(B)** Schema of constructs used for CAR T cells (I) and tumor cells (II/III) for development of luciferase complementation assay. SP = signal peptide; TM = transmembrane region; trECD = truncated extracellular domain; ECD = extracellular domain; ICD = intracellular domain. **(C)** Luminescence of nLuc+cLuc+ CAR T cells. Data represent mean ± S.D. of three technical replicates and is representative of two independent experiments. **(D)** CMT during coculture of FMC63 CAR T cells expressing nLuc with K562 cells expressing full length (teal) or truncated (tr19, orange) CD19 fused to cLuc using CompLuc or flow cytometry after 1 hour at the indicated effector-target ratios. CMT using CompLuc was measured for a total of 2.5 hours at 1-minute intervals. Data represents best fit of three technical replicates. Boxed area represents histogram of anti-CD19/FITC staining of CAR T cells at a 1:1 effector-target ratio after 1 hour as measured by flow cytometry. **(E)** Area-under-curve quantification of luminescence in Fig. 2D. Data represent mean ± S.D. of three technical replicates. **(F)** CMT during coculture of ΔscFv or FMC63 CAR T cells expressing nLuc with K562 cells expressing full length CD19-cLuc using CompLuc or flow cytometry after 1 hour at the indicated effector-target ratios. CMT using CompLuc was measured for a total of 2.5 hours at 1-minute intervals. Data represents best fit of three technical replicates. Boxed area represents histogram of anti-CD19/FITC staining of CAR T cells at a 1:1 effector-target ratio after 1 hour as measured by flow cytometry. **(D-F)** Data is representative of at least three independent experiments. **(G)** Peak luminescence of FMC63 CAR T cells cocultured with K562 cells

234 expressing CD19-cLuc at a 1:1 effector-target ratio as determined by CompLuc. CAR T cells were pre-
235 treated with cytochalasin D for 1 hour at the indicated concentrations. **(H)** Survival of Raji-Fluc cells after a
236 16-hour coculture with FMC63 CAR T cells pre-treated with the indicated concentrations of cytochalasin D.
237 CMT values are normalized to a DMSO control. **(G/H)** Data represent mean ± S.D. of three technical
238 replicates. Data is representative of two independent experiments.
239

240 *Extracellular cathepsin B is a key driver of CAR-mediated trogocytosis*

241 CMT may be the result of incomplete target cell killing followed by the endocytosis of
242 target cell fragments, as suggested by the simultaneous effect of cytochalasin D on CMT
243 and CAR-mediated cytotoxicity (Fig. 3H). However, we hypothesized that, while the
244 molecular mechanisms driving target cell killing and trogocytosis may overlap, CMT could
245 in part be mechanistically distinct from cytotoxic function.

246 To identify functional systems that could be specifically involved in CMT but not
247 cytotoxicity, we explored the effect of inhibiting various processes at the T cell immune
248 synapse on CMT[22,39–42] (Fig. 4A). We found that inhibition of cathepsin B (CTSB) with the
249 small molecule inhibitor Ca-074-Me in FMC63 CAR T cells reduced CMT in a dose-
250 dependent manner as measured by CompLuc (Fig. 4B) without substantially altering CAR
251 T cell cytotoxicity (Fig. 4C). Using a membrane-impermeable inhibitor of CTSB (Ca-074),
252 we found that inhibition of extracellular CTSB alone is sufficient to prevent CMT (Fig. 4D).

253 CTSB is a ubiquitously expressed cysteine protease, primarily localized to lysosomal and
254 endosomal compartments under physiological conditions, where it is primarily involved in
255 protein degradation and turnover[43,44]. However, CTSB is also found in the cytosol and
256 exocytic vesicles, retains its catalytic activity at neutral pH[45], and has been shown to line
257 exocytic granules of cytotoxic T lymphocytes[46]. In addition to proteolytic degradation
258 within the endosome and lysosome, CTSB has been implicated in the degradation and
259 remodeling of components of the extracellular matrix, such as collagen and fibronectin,
260 thereby promoting the invasion and metastasis of tumor cells[45,47,48]. Similarly, CTSB may

261 contribute to the extraction of antigen-rich membrane fragments of target cells prior to
262 their transfer to CAR T cells.

263 To further support the potential role of extracellular CTSB produced by CAR T cells in
264 CMT, we next determined whether CTSB in CAR T cells is actively transported to the
265 immune synapse upon antigen contact. To this end, we generated FMC63 CAR T cells
266 expressing CTSB fused to mCherry and exposed these cells to immobilized CD19 (Fig.
267 4E). Specifically, we assessed intracellular CTSB trafficking in these cells using live-cell
268 confocal imaging after exposing CAR T cells to recombinant CD19 immobilized on a glass
269 slide. When assessing CTSB movement, we found that CTSB in FMC63 CAR T cells, but
270 not in ΔscFv CAR T cells, rapidly localized to the site of antigen contact (Fig. 4F, Suppl.
271 Fig. S1D), correlating with the timing of CMT as measured by CompLuc and flow
272 cytometry (Fig. 3F). Specifically, following exposure to CD19, CTSB in FMC63 CAR T
273 cells was significantly less dispersed throughout the cell ("axial dispersion," Fig. 4G)
274 indicating coordinated CTSB trafficking and localization significantly closer to the site of
275 antigen contact (Fig. 4H) compared to ΔscFv CAR T cells. These findings suggest that
276 CTSB is actively and rapidly transported to the immune synapse upon antigen contact
277 and that its subsequent secretion by CAR T cells contributes to CMT.

278

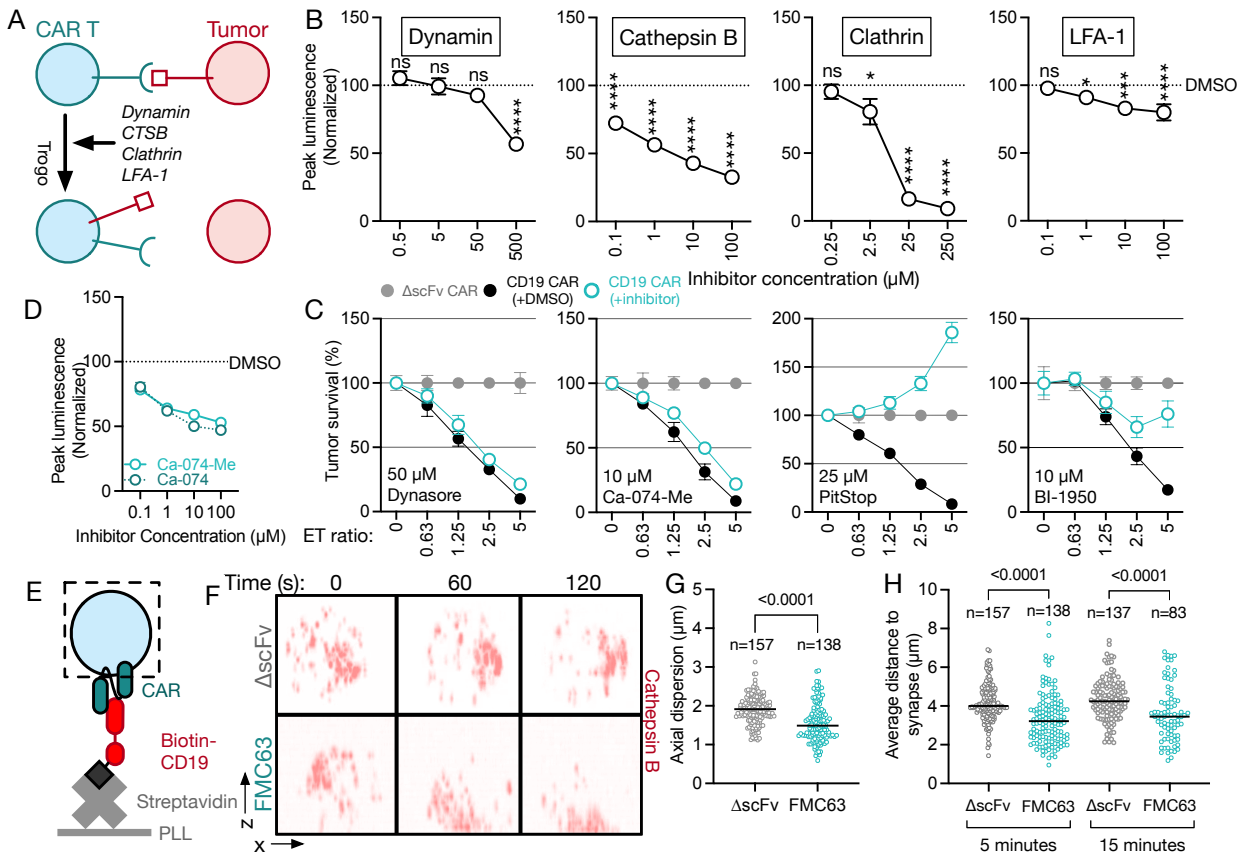


**Figure 4: Extracellular cathepsin B is a key driver of CAR-mediated trogocytosis. (A)** Schema of potential modulators of CMT. **(B)** Peak luminescence as determined by CompLuc of FMC63 CAR T cells treated with inhibitors of the indicated proteins cocultured with K562 cells expressing CD19-cLuc at a 1:1 effector-target ratio. Values are normalized to DMSO/vehicle control. Data represent mean ± S.D. of three technical replicates. Data is representative of three independent experiments. **(C)** Survival of Raji-Fluc cells after 16-hour coculture with FMC63 CAR T cells treated with inhibitors of the indicated proteins at a single concentration. Tumor survival was measured using a luciferase-based cytotoxicity assay. Data represent mean ± S.D. of three technical replicates. Data is representative of two independent experiments. **(D)** Peak luminescence as determined by CompLuc of FMC63 CAR T cells cocultured with K562 cells expressing CD19-cLuc at a 1:1 effector-target ratio. FMC63 CAR T cells were pre-treated with the indicated concentrations of Ca-074-Me (membrane-permeable) or Ca-074 (membrane-impermeable). Values are normalized to DMSO/vehicle control. Data represent mean ± S.D. of three technical replicates. Data is

293 representative of three independent experiments. **(E)** Schema of imaging assay setup used to assess
294 cathepsin B (CTSB) localization to the immune synapse. Biotinylated CD19 was immobilized on plate-
295 bound NeutrAvidin. ΔscFv or FMC63 CAR T cells expressing CTSB-mCherry were added to slides and
296 imaged using confocal microscopy. **(F-H)** ΔscFv or FMC63 CAR T cells expressing CTSB-mCherry were
297 imaged by spinning disk confocal imaging after exposure to CD19 immobilized on glass slides at different
298 time points. **(F)** Side (x-z) view of the distribution of CTSB-mCherry (red) at the indicated time points. The
299 bottom of each box is aligned to the interface between the glass slide and the T cell. **(G)** Axial dispersion
300 or **(H)** average distance of CTSB to the site of antigen contact. Data represent values from individual cells
301 fixed 5 or 15 minutes after exposure to recombinant CD19. Numbers represent cells analyzed for each
302 condition. **(G/H)** Statistical significance was determined by two-tailed Student's *t*-test. **(F-H)** Data is
303 representative of at least two independent experiments.
304

305 *Cystatin abundance controls CTSB activity and CMT*

306 CTSB is ubiquitously expressed across tissues and cell types, and its activity is regulated
307 through a network of endogenous protease inhibitors called cystatins[49]. Cystatin A
308 (CSTA) has been described as the main regulator of CTSB activity[50]. Like Ca-074, CSTA
309 inhibits CTSB through insertion of a hydrophobic wedge into the active-site cleft of
310 CTSB[51] (Fig. 5A). To determine if CSTA abundance directly regulates CMT in CAR T
311 cells, we engineered FMC63 CAR T cells to stably overexpress CSTA ($CAR_{CSTA}$, Fig. 5B).
312 We confirmed that CSTA overexpression led to significantly increased levels of CSTA
313 protein in CAR T cells (Fig. 5C), which resulted in reduced CTSB activity (Fig. 5D) without
314 altering *in vitro* CAR T cell expansion (Suppl. Fig. S4A/B), phenotype (Suppl. Fig S4C/D),
315 or cytokine secretion (Suppl. Fig. S4E). It has previously been shown that $CTSB^{KO}$ mice
316 are viable, suggesting that loss of CTSB activity may not cause major toxicity[52–55] . To
317 determine if CSTA overexpression by engineered T cells causes toxicity, we treated NRG
318 mice with CAR T cells overexpressing human CSTA (hCSTA) or mouse CSTA (mCSTA,
319 Suppl. Fig. S5A-D) and found that CSTA overexpression did not result in weight loss or
320 changes in major tissue architecture (Suppl. Fig. S5E-F). When co-cultured with tumor
321 cells, CD19 $CAR_{CSTA}$ cells showed equivalent short-term anti-tumor activity compared to
322 conventional CAR T cells (Fig. 5E, Suppl. Fig. S6A) whereas BCMA $CAR_{CSTA}$ cells
323 showed slightly improved short-term anti-tumor activity (Suppl. Fig. S6B). When co-
324 cultured with $CD19^+$ or $BCMA^+$ K562 cells, we observed significantly reduced CMT in
325 $CAR_{CSTA}$ cells as measured by CompLuc (Fig. 5F/G, Suppl. Fig. S6C/D) despite
326 comparable CAR T cell activation (Suppl. Fig. S6E). CMT was similarly reduced when

327 overexpressing a truncated $CSTA_{1-57}$ containing the hydrophobic wedge (Suppl. Fig S6F)
328 or the closely related protein cystatin B[56] (Suppl. Fig S6G-I). $CAR_{CSTA}$ T cells cocultured
329 with relevant hematologic or solid tumor cell lines showed reduced antigen transfer to
330 CAR T cells (Fig. 5H-J, Suppl. Fig. S6J-M) and antigen loss on tumor cells (Fig. 5K-M,
331 Suppl. Fig. S6N), suggesting inhibition of CMT at the antigen extraction step. This CSTA-
332 mediated inhibition of CMT resulted in significantly increased CD19 and BCMA CAR T
333 cell numbers after short-term exposure to tumor cells *in vitro* (Fig. 5N/O, Suppl. Fig. S6O).
334 To explore whether CSTA overexpression would be effective in a primary tumor cell
335 model, we cocultured CAR or $CAR_{CSTA}$ T cells with primary tumor cells from a patient with
336 B-cell acute lymphoblastic leukemia (B-ALL) and found that CSTA overexpression
337 significantly reduced CMT (Fig. 5P/Q) and increased CAR T cell numbers (Fig. 5R) in this
338 setting as well. These data demonstrate that, in short-term co-cultures with tumor cells,
339 CSTA overexpression significantly reduces CMT and increases CAR T cell survival.

340 We hypothesized that this effect on CAR T cell survival in short-term co-cultures could
341 also lead to increased long-term CAR T cell persistence and anti-tumor activity of
342 $CAR_{CSTA}$ T cells. We therefore next performed a serial cytotoxicity assay to determine
343 $CAR_{CSTA}$ T cell anti-tumor activity over an extended period of time (Fig. 6A). We found
344 that $CAR_{CSTA}$ T cells significantly prolonged tumor control (Fig. 6B) and observed
345 increased CAR T cell numbers over time (Fig. 6C). In an *in vivo* B-ALL tumor model (Fig.
346 6D), we observed tumor control in all groups treated with CD19-targeting CAR T cells
347 (Fig. 6E, Suppl. Fig. S7A) and again found significantly increased $CAR_{CSTA}$ T cell numbers
348 (Fig. 6F). When analyzing the phenotype of these persisting CAR T cells, we found that

349 CSTA overexpression did not significantly alter T cell subset composition (Fig. 6G). We
350 next explored expression of exhaustion markers in CAR T cells from *in vitro* serial
351 cytotoxicity and *in vivo* experiments. We found that, despite their substantially increased
352 persistence in both experiments, $CAR_{CSTA}$ cells showed significantly increased levels of
353 exhaustion (Fig. 6H, Suppl. Fig. S7B). To explore potential causes of this increased
354 exhaustion, we next performed bulk RNA sequencing of FMC63 CAR and $CAR_{CSTA}$ T
355 cells at the end of production. We found that CSTA overexpression resulted in the
356 spontaneous upregulation of Cytokine-Inducible SH2 containing protein (CISH), which
357 has previously been implicated as a key driver of CAR T cell exhaustion (Fig. 6I). To
358 determine if this upregulation of CISH could have caused the increased exhaustion of
359 $CAR_{CSTA}$ T cells, we next established an efficient CRISPR/Cas9-mediated CISH knockout
360 (Suppl. Fig. S7C/D). $CISH^{KO}$ did not result in changes to T cell subset composition at the
361 end of production (Suppl. Fig. S7E) and did not affect inhibition of CMT by CSTA
362 overexpression (Suppl. Fig. S7F-H) indicating that the effect of CSTA on CMT is not
363 mediated by CISH. We next performed a serial cytotoxicity assay using $CAR_{CSTA}$ cells
364 with and without $CISH^{KO}$ (Fig. 6J) and found that $CISH^{KO}$ significantly prolonged tumor
365 control and further increased CAR T cell persistence over time (Fig. 6K/L). In addition,
366 $CISH^{KO}$ almost entirely prevented exhaustion in CSTA-expressing CAR T cells in vitro
367 (Fig. 6M/N), indicating that CSTA-induced upregulation of CISH caused the increased
368 levels of exhaustion in $CAR_{CSTA}$ cells. We validated this finding in the same *in vivo* model
369 described above and again observed complete tumor control and increased persistence
370 in $CAR_{CSTA}$ $CISH^{KO}$ CAR T cells (Fig. 6O, Suppl. Fig. S7I). We next hypothesized that

371 CMT could be more pronounced in the solid tumor setting due to the higher density of
372 tumor cells leading to more extensive antigen transfer and fratricide. We therefore
373 established a solid tumor *in vivo* model by intratibial implantation of A673 Ewing sarcoma
374 cells engineered to express CD19 (Fig. 6P). This model was characterized by rapid
375 localized tumor growth and efficient tumor control by systemically injected FMC63 and
376 $CAR_{CSTA}$ $CISH^{KO}$ CAR T cells (Fig. 6Q, Suppl. Fig. S7J). In this model, we found that
377 CSTA expression did not alter CAR T cell numbers in the peripheral blood (Fig. 6R) but
378 substantially increased intratumoral $CAR_{CSTA}$ T cell numbers indicating that CSTA
379 overexpression does not negatively affect tumor infiltration by CAR T cells (Fig. 6S) and
380 instead efficiently prevents intratumoral CAR T cell fratricide. Exhaustion and phenotype
381 of $CAR_{CSTA}$ $CISH^{KO}$ cells was comparable to FMC63 CAR T cells indicating that $CISH^{KO}$
382 robustly prevents CSTA-mediated exhaustion in solid and hematologic settings (Fig.
383 6T/U, Suppl. Fig. S7K).

384 Taken together, these data indicate that CSTA overexpression leads to significantly
385 reduced CMT, as well as increased long-term CAR T cell persistence and tumor control.
386 CSTA-mediated induction of exhaustion via CISH could be overcome by simultaneous
387 $CISH^{KO}$ further enhancing functional CAR T cell persistence.
388

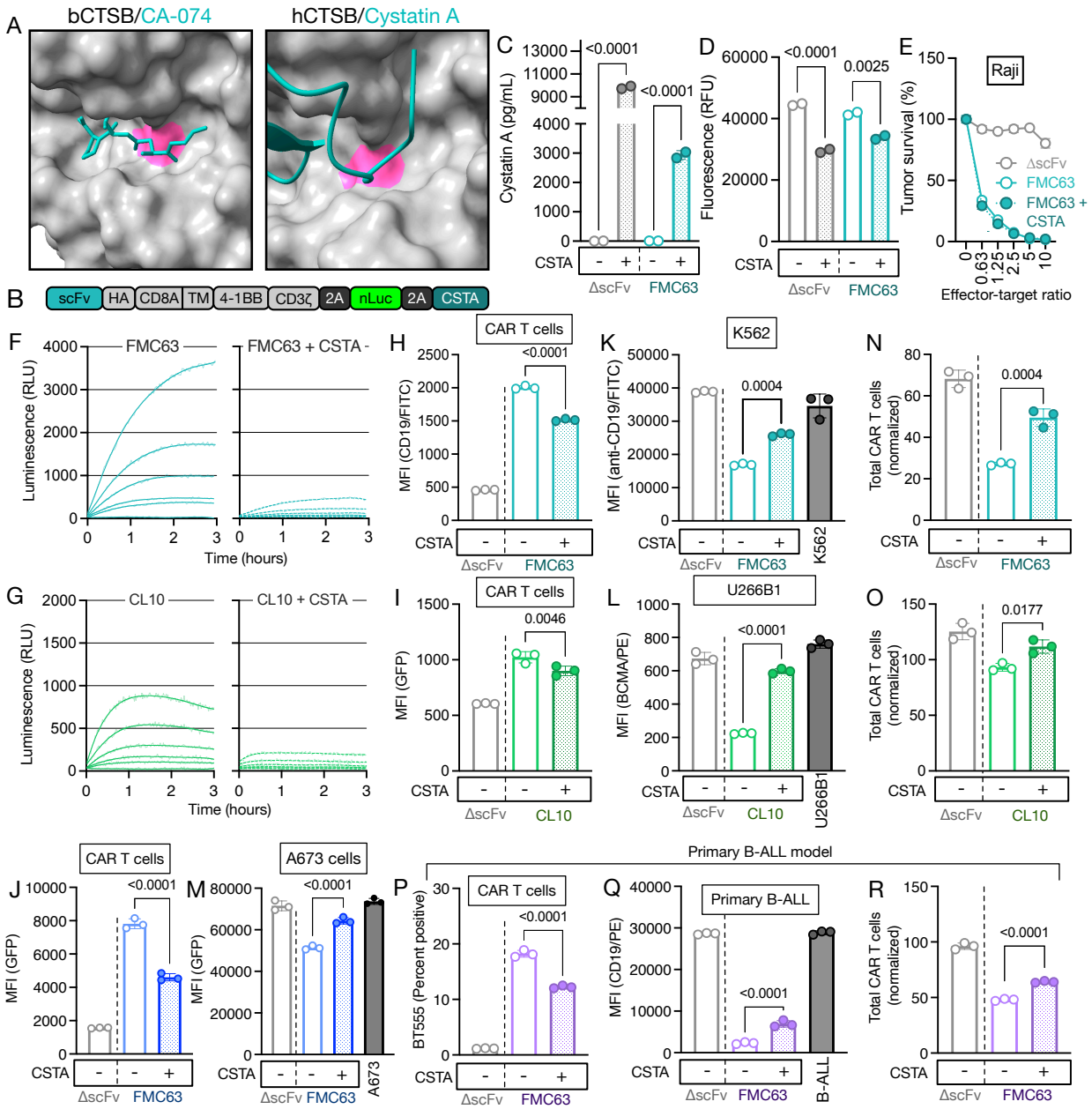


**Figure 5: Cystatin abundance controls CTSB activity and CMT. (A)** Crystal structures of bovine cathepsin B in complex with Ca-074 (left, PDB: 1QDQ) and human cathepsin B in complex with cystatin A (right, PDB: 3K9M). The active site cysteine of cathepsin B is shown in pink; Ca-074 and cystatin A are shown in teal. **(B)** Schema of construct used for production of $CAR_{CSTA}$ T cells. **(C)** Levels of CSTA in CAR or $CAR_{CSTA}$ T cells measured by ELISA. Data represent mean ± S.D. of two technical replicates. **(D)** Cathepsin B activity in CAR or $CAR_{CSTA}$ T cells measured by fluorescence-based CTSB activity assay. Data

396 represent mean ± S.D. of two technical replicates. **(C/D)** Data is representative of two independent
397 experiments. **(E)** Survival of Raji-Fluc cells after a 16-hour coculture with FMC63 CAR or $CAR_{CSTA}$ T cells
398 at the indicated effector-target ratios. Data represent mean ± S.D. of three technical replicates. Data is
399 representative of at least three independent experiments using cells produced from three healthy donors.
400 **(F)** CMT of FMC63 CAR or $CAR_{CSTA}$ T cells as determined by CompLuc using K562 cells expressing CD19-
401 cLuc after 3 hours. Data is representative of three independent experiments using cells produced from
402 three independent donors. **(G)** CMT in BCMA CAR or $CAR_{CSTA}$ T cells as determined by CompLuc using
403 K562 cells expressing BCMA-GFP-cLuc after 3 hours. Data is representative of three independent
404 experiments. **(F/G)** Data represents best fit of three technical replicates. **(H)** CD19 transfer to CAR T cells
405 following a 30-minute coculture of FMC63 CAR or $CAR_{CSTA}$ T cells with K562 cells expressing CD19-cLuc
406 at a 0.5:1 effector-target ratio as determined by flow cytometry. Data is representative of at least three
407 independent experiments using cells produced from three healthy donors. **(I)** BCMA-GFP transfer to CAR
408 T cells following a 2-hour coculture of BCMA CAR or $CAR_{CSTA}$ T cells and K562 cells expressing BCMA-
409 GFP-cLuc at a 1:1 effector-target ratio as determined by flow cytometry. Data is representative of three
410 independent experiments. **(J)** GFP transfer to CAR T cells following a 1-hour coculture with A673 cells
411 engineered to express a CD19-GFP fusion protein at a 1:1 effector target ratio. **(K)** CD19 loss on tumor
412 cells following a 30-minute coculture of FMC63 CAR or $CAR_{CSTA}$ T cells and K562 cells expressing CD19-
413 cLuc at a 0.5:1 effector-target ratio as determined by flow cytometry. Data is representative of at least three
414 independent experiments using cells produced from three healthy donors. **(L)** BCMA loss on U266B1 tumor
415 cells following a 2-hour coculture of BCMA CAR or $CAR_{CSTA}$ T cells and K562 cells expressing BCMA-GFP-
416 cLuc at a 1:1 effector-target ratio as determined by flow cytometry. Data is representative of three
417 independent experiments. **(M)** GFP loss on A673 tumor cells following a 1-hour coculture of FMC63 CAR
418 or $CAR_{CSTA}$ T cells and A673 cells expressing CD19-GFP at a 1:1 effector-target ratio as determined by
419 flow cytometry. **(J/M)** Data is representative of two independent experiments using cells produced from
420 three healthy donors. **(N)** Total CAR T cells following a 30-minute coculture of FMC63 CAR or $CAR_{CSTA}$ T
421 cells and K562 cells expressing CD19-cLuc at a 0.5:1 effector-target ratio as determined by flow cytometry.
422 Data is representative of at least three independent experiments using cells produced from three healthy

423 donors. **(O)** Total CAR T cells following a 2-hour coculture of BCMA CAR or $CAR_{CSTA}$ T cells and K562 cells
424 expressing BCMA-GFP-cLuc at a 1:1 effector-target ratio as determined by flow cytometry. Data is
425 representative of three independent experiments. **(N/O)** CAR T cell numbers are normalized to wells
426 containing only CAR T cells using counting beads. **(P)** CD19 transfer to CAR T cells following a 1-hour
427 coculture of FMC63 CAR or $CAR_{CSTA}$ T cells and primary B cell acute lymphoblastic leukemia (B-ALL) cells
428 at a 1:1 effector-target ratio as determined by flow cytometry. **(Q)** CD19 loss on primary B-ALL cells
429 following a 1-hour coculture of FMC63 CAR or $CAR_{CSTA}$ T cells and primary B-ALL cells at a 1:1 effector-
430 target ratio as determined by flow cytometry. **(R)** Total CAR T cells following a 1-hour coculture of FMC63
431 CAR or $CAR_{CSTA}$ T cells and primary B-ALL cells at a 1:1 effector-target ratio as determined by flow
432 cytometry. **(Q-R)** Data is representative of three independent experiments. **(H-R)** Statistical significance
433 was determined by one-way ANOVA.
434

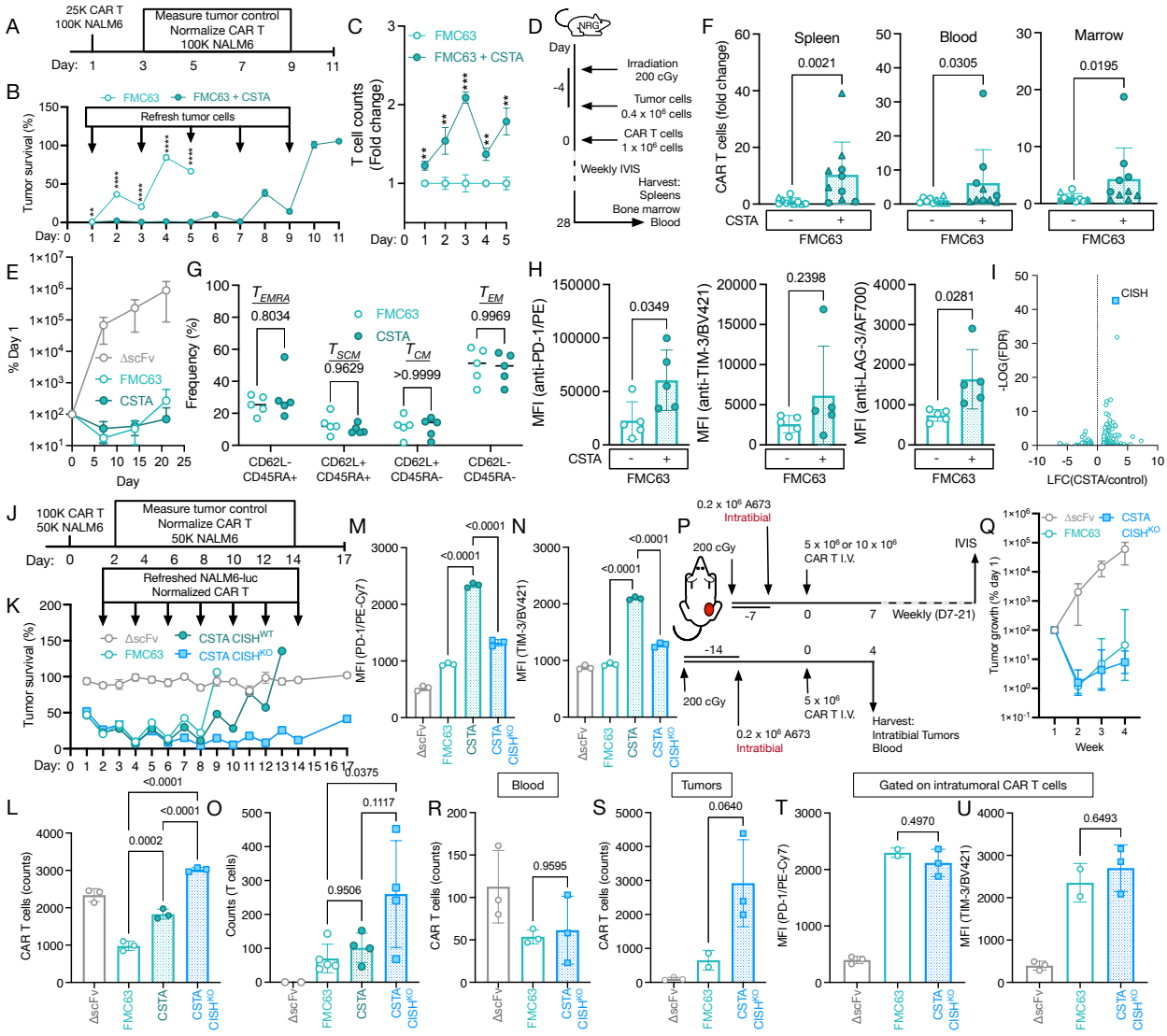


**Figure 6: Cystatin A overexpression improves long-term CAR T cell persistence. (A)** Schema of *in vitro* experiment to determine long-term CAR T cell persistence and antitumor activity. **(B)** Survival of CD19-GFP-expressing NALM6-Fluc cells at a 0.5:1 effector-target ratio using a luminescence-based cytotoxicity assay. Data indicates mean ± S.D. from three technical replicates. Tumor survival was normalized to untreated tumor cells. Data is representative of two independent experiments. Statistical significance comparing FMC63 CAR and $CAR_{CSTA}$ T cells was determined by multiple two-tailed Student's *t*-tests**. (C)** FMC63 CAR and $CAR_{CSTA}$ T cell counts on D1-5 of the *in vitro* serial coculture described in Fig. 6A. Data represent mean ± S.D. of 3 technical replicates and is representative of two independent experiments. Statistical significance comparing FMC63 CAR and $CAR_{CSTA}$ T cells was determined by multiple two-tailed

445 Student's *t*-tests**. (D)** Schema of *in vivo* experiment to measure NALM6 tumor control and CAR T cell
446 persistence. **(E)** Tumor burden in mice bearing systemic NALM6-Fluc tumors and treated with ΔscFv or
447 FMC63 CAR or $CAR_{CSTA}$ T cells as determined by *in vivo imaging system (IVIS).* Data represent mean ±
448 S.D. of 5 mice per group. Statistical significance was determined by two-way ANOVA. **(F)** Quantification of
449 CAR T cells in murine spleen, peripheral blood, and bone marrow as determined by flow cytometry. Data
450 represent mean ± S.D. of 10 mice pooled from two independent experiments, with experiments denoted by
451 symbol. Data were normalized to the average of the respective experiment's $CSTA^{-}$ condition and are
452 expressed as fold change. Statistical significance was determined by two-tailed Student's *t*-test. **(G)**
453 Phenotype of FMC63 CAR/$CAR_{CSTA}$ T cells isolated from murine blood as determined by flow cytometry.
454 Statistical significance was determined by two-way ANOVA. **(H)** PD-1, TIM-3, and LAG-3 expression on
455 FMC63 CAR or $CAR_{CSTA}$ T cells isolated from murine blood as determined by flow cytometry. Statistical
456 significance was determined by two-tailed Student's *t*-test. **(G/H)** Data represent mean ± S.D. of 5 mice per
457 group. **(I)** Differential mRNA expression in sorted FMC63 CAR and $CAR_{CSTA}$ T cells after manufacturing as
458 determined by bulk RNA sequencing. Data is representative of cells from two independent productions. **(J)**
459 Schema of *in vitro* experiment to determine long-term CAR T cell persistence and antitumor activity. **(K)**
460 Survival of NALM6-Fluc cells at a 2:1 effector target ratio using a luminescence-based serial cytotoxicity
461 assay. On Days 2, 4, 6, 8, 10, 12, and 14 CAR T cells were normalized and fresh tumor cells were added.
462 Statistical significance was determined by two-way ANOVA. **(L)** Total CAR T cells on Day 10 of the *in vitro*
463 serial coculture described in Fig. 6J. **(M)** PD-1 expression on CAR T cells on Day 5 of *in vitro* serial coculture
464 described in Fig. 6J. **(N)** TIM-3 expression on CAR T cells on Day 5 of *in vitro* serial coculture described in
465 Fig. 6J. **(K-N)** Data represent mean ± S.D. of three technical replicates and is representative of two
466 independent experiments. **(O)** Quantification of CAR T cells in bone marrow 28 days after intravenous
467 treatment with the indicated CAR T cell conditions as determined by flow cytometry. Data represent mean
468 ± S.D. of 2-5 mice per group. Statistical significance was determined by one-way ANOVA. **(P)** Schema of
469 *in vivo* experiment to measure solid tumor control and CAR T cell infiltration into solid tumors. **(Q)** Tumor
470 burden in mice bearing intratibial CD19-expressing A673-Fluc tumors and treated intravenously with ΔscFv
471 or FMC63 CAR $CISH^{WT}$ or $CAR_{CSTA}$ $CISH^{KO}$ T cells as determined by *in vivo imaging system (IVIS).* Data

472 represent mean ± S.D. of 3-4 mice per group. **(R)** Quantification of CAR T cells in peripheral blood four
473 days after treatment with the indicated CAR T cell conditions as determined by flow cytometry (n = 2-3 per
474 group). Statistical significance was determined by one-way ANOVA. **(S)** Quantification of CAR T cells in
475 intratibial A673 tumors four days after treatment with the indicated CAR T cell conditions as determined by
476 flow cytometry (n = 2-3 per group). Statistical significance was determined by one-way ANOVA. **(T)** PD-1
477 and **(U)** TIM-3 levels on intratumoral CAR T cells four days after CAR T cell injection as determined by flow
478 cytometry. Statistical significance was determined by one-way ANOVA. **(R-U)** Data represent mean ± S.D.
479 of 2-3 mice per group.

480 **Discussion**

481 CAR T cells have revolutionized cancer immunotherapy, but most patients receiving CAR
482 T cell therapy relapse within 5 years of treatment[12,57,58]. Several mechanisms driving
483 relapse after CAR T cell therapy have been described, including CAR T cell-mediated
484 trogocytosis (CMT). CMT, the extraction of tumor antigen from the tumor cell and its
485 subsequent incorporation into the CAR T cell membrane, is modulated by CAR affinity for
486 target antigen[23], actin rearrangement[22,39], cholesterol metabolism[59], and the CAR
487 transmembrane domain[60]. CMT has previously been shown to result in the emergence of
488 antigen-negative tumor cells[22–24] and had been hypothesized to cause CAR T cell
489 fratricide as well as CAR T cell exhaustion through persistent cis signaling[61]. Previous
490 studies have demonstrated the presence of tumor antigen on CAR T cells following co-
491 culture with tumor cells and that the presence of trogocytosed antigen correlates with
492 increased apoptotic markers and exhaustion[22–24]. However, it remained unknown if this T
493 cell dysfunction was indeed caused by CMT. In this study, we sought to determine if the
494 presence of trogocytosed antigen causes CAR T cell dysfunction and to uncover
495 molecular modulators of CMT to improve our understanding of the trogocytic process.

496 In this study, we demonstrate that CAR T cell fratricide and exhaustion can be reversed
497 through selective degradation of trogocytosed antigen on the CAR T cells, indicating that
498 trogocytosed antigen is indeed directly causing CAR T cell dysfunction. We show that this
499 trogocytosed antigen degrader (TAD) approach is feasible when targeting an antigen-
500 GFP fusion protein as well as the unmodified endogenous antigen (CD19) by using
501 endogenous protein domains binding to the target antigen's intracellular domain. The

502 TAD protein targeting endogenous CD19 ($TAD_{CD19}$) relies on the established high-affinity
503 interaction of the Lyn kinase SH2 domain with the intracellular domain of CD19[36].
504 However, SH2 domains can be involved in multiple signaling pathways with their activity
505 being highly context-dependent[62–64]. It is therefore possible that $TAD_{CD19}$ could bind to
506 proteins other than CD19. Because of this possibility, we mainly relied on the use of
507 $TAD_{GFP}$, which relies on a validated protein-protein interaction and is unlikely to result in
508 similar off-target effects[32]. If TAD-mediated targeting of an endogenous antigen is desired
509 in the absence of target-specific endogenous binding domains, protein binders could be
510 generated de novo, analogous to the GFP-specific VHH domain used in this study. Future
511 work focusing on TAD-based approaches using endogenous binding domains will have
512 to carefully consider potential off-target reactivity.

513 In this study, we found that the cysteine protease cathepsin B (CTSB) produced by CAR
514 T cells is essential for CMT but dispensable for tumor cell killing. We demonstrate that
515 CTSB produced by CAR T cells rapidly localizes to the immune synapse upon antigen
516 stimulation and that extracellular CTSB confers antigen extraction from tumor cells. A role
517 of extracellular CTSB in the processing of cellular material is in line with prior studies
518 describing the involvement of tumor-derived CTSB in the degradation and remodeling of
519 components of the extracellular matrix, enabling tumor metastasis[45,47,48]. We further show
520 that CTSB activity in CAR T cells is tightly regulated through the abundance of cystatins,
521 a class of endogenous protease inhibitors[49,51]. We found that overexpression of both
522 cystatin A and cystatin B potently inhibited CTSB in CAR T cells. While the small molecule
523 inhibitors used throughout this study have been shown to be specific for CTSB[65,66], the

524 more robust inhibition of CMT by cystatins, which are able to inhibit a range of cathepsins,
525 including cathepsin L and H, could indicate a role of other cathepsins in CMT[49,51].

526 In principle, constitutive overexpression of CSTA to limit CMT could cause toxicity through
527 systemic inhibition of CTSB or other proteases[67]. However, it has been shown previously
528 that $CTSB^{KO}$ mice are viable and appear indistinguishable from $CTSB^{WT}$ mice[52–55]. In
529 addition, we found that mice treated with $CAR_{CSTA}$ T cells exhibit no overt signs of toxicity.
530 While constitutive overexpression of CSTA appears to be relatively safe, additional work
531 will need to be performed in relevant model systems to confirm our initial observations. In
532 case toxicities are observed, the safety of CSTA overexpression could be increased by
533 using a conditional expression system that initiates CSTA expression upon CAR target
534 recognition or recognition of a separate tissue-specific antigen[68,69].

535 In this study, we specifically focused on the role of CAR T cell-derived factors on CMT.
536 However, CTSB is expressed by both T cells and tumor cells. Using the covalent small
537 molecule CTSB inhibitor Ca-074-Me, we show that specific inhibition on CAR T cell-
538 derived CTSB directly causes CMT. However it is possible that tumor-derived CTSB also
539 contributes to this process and further work is needed to comprehensively explore this
540 possibility.

541 Increased levels of cystatins other than CSTA, such as cystatin F, a type II cystatin and
542 inhibitor of cathepsins C, L, and H, have been found to decrease cytotoxicity in NK cells
543 and T cells[70,71], raising the question of how CSTA overexpression may affect CAR T cell
544 function and tumor control. In this study, we observed no differences in short-term *in vitro*
545 cytotoxicity and cytokine secretion between FMC63 CAR and $CAR_{CSTA}$ cells. However,

546 we observed substantially increased long-term tumor control by $CAR_{CSTA}$ cells *in vitro*,
547 which was also associated with significantly increased CAR T cell numbers in
548 hematologic and solid tumor models *in vitro* and *in vivo*. Increased tumor control by
549 $CAR_{CSTA}$ cells is in line with previous studies which showed that inhibiting CMT using
550 inhibitory CARs[24], combinatorial targeting[22], or altering cholesterol metabolism[72] can
551 increase anti-tumor activity. However, in long-term *in vitro* and *in vivo* experiments, we
552 observed significant upregulation of exhaustion markers on $CAR_{CSTA}$ T cells. Analyzing
553 the pre-infusion product, we found that $CAR_{CSTA}$ T cells showed spontaneous
554 upregulation of cytokine-inducible SH2-containing protein (CISH), a known negative
555 regulator of T cell activation[73,74]. By including a CISH knockout step during $CAR_{CSTA}$
556 production, we were able to show that the CSTA-induced exhaustion was mediated by
557 CISH, which is in line with recent studies showing that CISH can be a major driver of CAR
558 T cell exhaustion in some contexts [75,76] . Our work serves as an initial proof-of-concept
559 showing that protease inhibition is an effective approach to limit CMT but additional work
560 will be needed to better understand how CSTA alters CISH expression and whether it is
561 possible to further separate the beneficial effects of CSTA overexpression from those
562 conferring increased exhaustion.

563 In addition to investigating the effects of CMT on CAR T cell persistence and function, we
564 show here that antigen density is substantially lowered on tumor cells through CMT and
565 that CMT is detectable in patients treated with CAR T cells. However, it remains unclear
566 how much transient antigen loss observed after CMT contributes to clinical antigen
567 escape. Monitoring CMT with high temporal resolution *in vivo* through continuous

568 sampling could help to answer this question by elucidating the extent of CMT-mediated
569 antigen loss. In addition, high-resolution imaging of *in vitro* cocultures with tumor cells
570 and CAR T cells may allow visualization of tumor cells following CMT to determine if
571 antigen loss protects these cells temporarily from CAR T cell-mediated killing.

572 Trogocytosis is a highly variable phenomenon and can be affected by several factors
573 including tumor antigen density[22] , target affinity[23], CAR structure[22,60] , and target cell
574 type. We observed substantial variability in CMT when analyzing the peripheral blood of
575 patients receiving CAR T cell therapy, and recent work also shows variability of CMT in
576 mice[60]. It remains an open question why CMT varies between patients and larger clinical
577 immunomonitoring trials will be needed to conclusively address this question.

578 Our study primarily focused on approaches targeting the two clinically validated CAR T
579 cell antigens CD19 and BCMA approved for the treatment of several hematologic
580 malignancies; however, we also show that CMT can be observed in solid malignancies
581 when targeting different, previously validated CAR antigens. While CMT appears to occur
582 across CAR target antigens, it remains an open question whether transfer of functionally
583 essential and/or tumorigenic proteins, the loss of which would result in rapid target cell
584 death, would be equally susceptible to this process. In the solid tumor setting, exhaustion-
585 driven T cell dysfunction is generally more pronounced[77,78] and CMT may play a key role
586 due to a denser tumor microenvironment and limited T cell mobility, which may favor more
587 extensive intratumoral fratricide. High-resolution intratumoral imaging may provide critical
588 insights into CMT dynamics to inform future strategies to reduce the impact of this
589 process.

590 In conclusion, we show that CMT directly causes CAR-mediated fratricide and exhaustion
591 and that CTSB is essential for CMT. CTSB activity is controlled by the abundance of
592 endogenous human cystatins and cystatin overexpression results in significantly reduced
593 CMT, fratricide, exhaustion, and increased CAR T cell persistence and anti-tumor activity.
594 CSTA overexpression is an effective approach to limit the negative consequences of CMT
595 but requires additional engineering, such as CISH knockout, to prevent CSTA-mediated
596 CAR T cell exhaustion. Our findings provide evidence that CMT is mechanistically distinct
597 from cytotoxic function in CAR T cells and support the rational targeting of this resistance
598 mechanism in CAR T cells.

599 **MATERIALS AND METHODS**

600 **Study approval**

601 All recombinant DNA and biosafety work was approved by the institutional biosafety
602 committees at University of Maryland, Baltimore (protocol IBC-6040). Animal experiments
603 were approved by the institutional animal care and use committee at the University of
604 Utah (protocol 18-1104).

605 **Cell lines and primary human cells**

606 Raji, NALM6, Daudi, DB, Toledo, MM.1S, RPMI8226, U266B1, K562, A673, TC-71, and
607 Phoenix-AMPHO cells were purchased from the American Type Culture Collection
608 (ATCC) and cultured according to ATCC instructions. Lenti-X 293T cells were purchased
609 from Takara and cultured according to the manufacturer's instructions. Cell lines were
610 authenticated by their respective supplier. Healthy donor buffy coats were obtained from
611 the New York Blood Center. PBMCs from healthy donors were isolated from buffy coats
612 by density gradient using FillPaque (GE) as previously described[27,30]. Primary human T
613 cells were cultured in AIM-V medium (Invitrogen 12055-083) supplemented with 5%
614 Human serum (Sigma H4522-100ML), 1% Pen/Strep (Thermofisher 15140-122) (T cell
615 media), and 40 IU IL-2 (R&D Systems #202-IL-10). All cells were cultured at 37°C, 5%
616 CO2.

617 **Vector constructs**

618 All vectors generated for this study were produced by Twist Biosciences. FMC63-nLuc
619 contains the CD19-specific scFv fragment FMC63 [79]. All CAR constructs contain the
620 CD8α hinge/transmembrane domain, 4-1BB costimulatory domain, and CD3z domain.

621 For some constructs, the full-length sequence of human cystatin A (UniProt, P01040) was
622 synthesized and cloned downstream of the respective CAR and nLuc fragment separated
623 by a P2A sequence (Twist Bioscience). DNA was isolated using Endofree Plasmid Maxi
624 Kit (Qiagen 12362) following the manufacturer's protocol. Plasmid concentration was
625 measured using a NanoDrop One instrument (Thermo). All DNA constructs were stored
626 at -20°C.

627 **Clinical data**

628 Whole blood was drawn from patients receiving CAR T cell therapy 7-28 days after CAR
629 T cell injection. Peripheral blood mononuclear cells (PBMCs) were isolated by density
630 gradient using Ficoll Paque as previously described[27,30]. PBMCs were stained with anti-
631 hCD3, anti-hCD4, anti-hCD8, anti-CAR (Miltenyi #130-127-342), and anti-hCD19, anti-
632 hCD27, anti-hCD137, and 7-AAD and analyzed by flow cytometry. Samples were
633 collected under Institutional Review Board (IRB)-approved protocol 2043GCCC (IRB
634 H0091736, PI D. Atanackovic).

635 **Gamma retrovirus Production**

636 Gamma retrovirus was produced using Phoenix-AMPHO cells (ATCC, catalog no. CRL-
637 3213). Phoenix-AMPHO cells were transiently transfected with 16 $\mu$g of plasmid DNA
638 using Opti-MEM Reduced Serum Medium (Thermofisher, catalog no. 31985070) and
639 lipofectamine 2000 (Invitrogen 11668-019) according to manufacturer's instructions.
640 During transfection, cells were cultured in Dulbecco's Modified Eagle Medium (DMEM,
641 Thermofisher 11995073) supplemented with 10% FBS. Virus-containing supernatant was
642 filtered using Steriflip™ Sterile Disposable Vacuum Filter Units (Millipore Sigma

643 SEIM003M00). Virus was concentrated using Retro-X Concentrator (Takara, 631456).
644 The following day, concentrated virus was centrifuged at 1500 x g for 45 minutes at 4°C.
645 Supernatant was removed and concentrated virus was resuspended in 1.5 mL complete
646 T cell media.

647 **Transgenic T cell production and expansion**

648 CAR T cells were generated as previously described[23,27,30]. Buffy coats from three healthy
649 donors were obtained from the New York Blood Center and peripheral blood mononuclear
650 cells (PBMCs) were isolated using Ficoll-Paque and cryopreserved until use. PBMCs
651 were thawed and cultured overnight in complete T cell media. PBMCs were stimulated
652 for 2 days with anti-CD3/anti-CD28 T cell activation beads (Thermo, catalog no. 11131D)
653 in the presence of interleukin-2 (IL-2; 40 IU/ml; R&D Systems, catalog no. 202-IL-010) in
654 complete T cell media and incubated at 37°C, 5% $CO_2$. Bead-stimulated cells were
655 transferred to RetroNectin-coated (Takara) virus–containing plates and incubated
656 overnight. Transduction was repeated the next day before counting and diluting cells to
657 $0.4 \times 10^6$ cells/ml. After the second transduction, cells were grown for an additional 7 days
658 before removing beads using a DynaMag-15 magnet (Thermo Fisher Scientific). IL-2 was
659 replenished every 2 days to 40 IU/ml. Cells were frozen in 90% fetal bovine serum/10%
660 dimethyl sulfoxide and stored in liquid nitrogen. CAR T cell transduction efficiency and
661 phenotype were determined by flow cytometry. CAR T cells were washed with FACS
662 buffer and stained with antibodies targeting hCD3, HA, hCD4, hCD8, hCD95, hCD62L,
663 and hCD45RA. Because BCMA $CAR_{CSTA}$ T cells showed substantially lower transduction
664 efficiency than conventional BCMA CAR T cells, after production, we FACS sorted both

665 products following anti-HA (CAR) staining using a FACSAria cell sorter (BD) prior to
666 subsequent functional assays.
667 To generate CISH$^{KO}$ CAR T cells, on day 5, anti-CD3/CD28 T Activator beads (Thermo
668 Fisher) were removed from the transduced cells by magnetic separation. CRISPR
669 ribonucleoprotein (RNP) particles containing 25 $\mu$g Cas9 only (mock/WT) or Cas9 and
670 150 pmol synthetic TrueGuide gRNA (CISH target sequence: 5'-
671 GACAGCGUGAACAGGUAGCU-3') were prepared according to the manufacturer's
672 instructions (Thermo). 3 x $10^6$ cells were electroporated in the presence of CRISPR-RNPs
673 using the NEON electroporation system (Thermo) using the following settings: 1,600 V,
674 10 ms, 3 pulses. Following the electroporation, cells were transferred to prewarmed
675 media and incubated for 2 hours at 37°C. Following the incubation, new anti-CD3/CD28
676 T cell activation beads were added to the electroporated cells at a ratio of 3:1, and cells
677 were grown for an additional 6 days before removing beads using a DynaMag-15 magnet
678 (Thermo Fisher). IL-2 was replenished every 2 days to 40 IU/ml. Cells were frozen in 90%
679 FCS/10% DMSO and stored in liquid nitrogen.

680 **Imaging Substrate Preparation**

681 Eight-well chambers (Cellvis, catalog no. C8-1.5H-N) were used for all experiments. For
682 CAR T cell activation on CD19-coated surfaces, 8-well chambers were coated with 0.01%
683 poly-L-lysine (PLL) solution diluted in distilled water for 10 minutes at room temperature.
684 PLL was aspirated from each well, and the chambers were allowed to air-dry for 1 hour
685 at 37°C. PLL-coated dishes were then incubated overnight at 4°C with a 10 µg/mL
686 solution of NeutrAvidin (Thermo Scientific, catalog no. 31000) in 1x Dulbecco's

687 phosphate-buffered saline (DPBS). After overnight incubation, coated wells were washed
688 with 1x DPBS at room temperature and incubated at 37°C with a 10 µg/mL solution of
689 biotinylated human CD19 protein (ACRO Biosystems catalog no. CD9-H82E9) in DPBS
690 for 2 hours at 37°C. Prior to the experiment, coated wells were washed three times with
691 RPMI 1640 phenol red-free imaging medium. For coculture experiments, 8-well chambers
692 wells were incubated with 10 µg/mL fibronectin (MilliporeSigma, catalog no. 34-163-
693 11MG) in DPBS at room temperature for 1 hour prior to seeding with 293T cells stably
694 expressing CD19-GFP. 293T cells were seeded at a concentration of 5 x $10^5$ cells per
695 well in complete growth media, followed by an overnight incubation at 37°C, 5% $CO_2$.
696 Prior to imaging, wells were washed three times with warm complete imaging media,
697 consisting of a 1:1 ratio of RPMI 1640 supplemented with 5% fetal bovine serum (FBS)
698 and DMEM supplemented with 10% FBS. The washing process was performed thrice to
699 ensure removal of any residual media while leaving a known volume in the wells.

700 **Confocal Microscopy**

701 Confocal microscopy was conducted using an inverted microscope (Nikon Ti-E PFS,
702 Nikon Inc.) equipped with a 100× Silicone objective lens. Imaging was performed with a
703 Prime BSI camera (Photometrics). Image acquisition protocols were managed using
704 Nikon Elements software, and images were cropped in FIJI for further analysis. All live
705 cell imaging was done with imaging chambers placed in a stage-top Okolab Incubator
706 (Okolab S. R. L.) pre-equilibrated to 37°C with 5% $CO_2$. For live cell imaging on glass,
707 activated CAR T cells suspended in RPMI 1640 medium supplemented with 5% FBS
708 were deposited onto CD19-coated surfaces. Imaging was started between 3 to 6 minutes

709 after CAR T cells expressing CTSB-mCherry were added to a biotin-CD19-coated
710 coverslip. For each well, timelapse images of a 3D volume (planes with z spacing of 0.3
711 µm to span the cell from the top to the bottom) were acquired every 3 minutes for 60
712 minutes. For coculture experiments, imaging was started between 3 to 6 minutes after
713 CAR T cells expressing CTSB-mCherry were dropped onto a layer of 293T cells
714 expressing CD19-GFP seeded on a coverslip, at a concentration of 7 x $10^4$ cells per drop.
715 Brightfield imaging was used to identify cells attached to the apical surface of HEK293
716 cells. The synaptic plane between a CAR-T cell and a HEK293 cell was identified and
717 designated as the home plane for acquisition of Z-stack time-lapse movies. Two-channel
718 images using 488 nm and 561 nm lasers (for GFP and mCherry imaging respectively)
719 were acquired every 3 minutes for 1 hour and 15 minutes utilizing a Z-spacing of 0.3 or
720 0.6 µm, with brightfield images taken at the home plane.
721 Image analysis was carried out in MATLAB (Mathworks, Inc.) using custom scripts. The
722 plane of the synapse was determined using the actin channel. After background
723 subtraction, axial intensity gradients are estimated for every voxel of sufficient intensity
724 within the ROI. Below the cell, these gradients are typically positive due to the Airy pattern
725 of the PSF. The synapse is taken as the first plane for which the gradients are no longer
726 consistently positive.

727 **Estimating the average distance of CTSB to the synapse**

728 The center of fluorescence (COF) of CTSB is defined similarly to the center of mass. The
729 voxel positions are weighted by CTSB intensity after background subtraction and

730 thresholding to obtain the COF. The average CTSB distance is then calculated from the
731 axial (z) distance of the Cathepsin B COF to the plane of the synapse.

732 **Characterizing CTSB axial dispersion**

733 The axial dispersion is an estimate of the average distance of CTSB molecules to the
734 COF. The axial (z) distance of each voxel to the COF is determined, and the axial
735 dispersion is defined as the average of these distances weighted by CTSB intensity after
736 background subtraction and thresholding. Voxels with sufficiently low signal do not
737 contribute to the calculation due to the thresholding procedure.

738 **CTSB clustering at the synapse**

739 The pair auto-correlation function g(r) of CTSB is computed at the synapse using the actin
740 channel as a mask[80]. The actin channel is segmented by smoothing with a Gaussian filter,
741 generating an initial mask by applying k-means clustering (k = 2) after a log
742 transformation, and then applying morphological operations to connect and smooth the
743 initial mask. The clustering coefficient, $g_{ave}$, is computed by averaging over all radial bins
744 with 0.25 m or 0.5 m.

745 **CompLuc-based trogocytosis assay**

746 Transduced, cryopreserved nLuc+ CAR T cells were thawed and cultured in complete T
747 cell media supplemented with 40 IU IL-2 for 48 hours prior to use. nLuc-expressing CAR
748 T cells were cocultured with CD19-cLuc-expressing K562 tumor cells at the specified
749 effector-target ratios. CAR T cells and tumor cells were resuspended in Opti-MEM
750 reduced serum media. Live Cell Substrate (Promega, catalog no. N2011) was prepared

751 according to manufacturer's instructions. K562 tumor cells and prepared Live Cell
752 Substrate were added to wells of a black 96-well plate and luminescence was measured
753 to assess baseline luminescence. CAR T cells were added to appropriate wells and
754 luminescence was measured every minute for three hours at 37˚C. Luminescence was
755 measured using a Spark multi-mode plate reader (Tecan).

756 **Flow cytometry-based trogocytosis assay**

757 A flow-cytometry based trogocytosis assay was used to confirm results observed in
758 CompLuc, to assess CD19 or BCMA levels on CAR T cells and tumor cells, and to
759 quantify CAR T cells. 5 x $10^4$ target cells were seeded in wells of a 96-well round bottom
760 plate. Various ratios of CAR T cells produced from one of three healthy donors were
761 cocultured with target cells for 1 hour at 37˚C, 5% $CO_2$. Following coculture, cells were
762 resuspended by gentle pipetting and transferred to wells of a 96-well V bottom plate for
763 washing and staining. Cells were stained with Zombie violet or Zombie NIR fixable viability
764 dye, and antibodies for hCD3, HA, hCD19 or BCMA. When assessing exhaustion, cells
765 were stained with antibodies targeting PD-1, LAG-3, and TIM-3. When assessing
766 phenotype, cells were stained with antibodies targeting CD45RA and CD62L. Accucheck
767 counting beads (Life Technologies) were added to the cells for normalization. Samples
768 were acquired on an LSR II flow cytometer (BD) or an Aurora full-spectrum flow cytometer
769 (Cytek).

770 **Luciferase-based cytotoxicity assay**

771 To determine *in vitro* CAR T cell cytotoxicity, cell lines (Raji, NALM6, Daudi, Toledo
772 MM.1S, RPMI8226, U266B1) were transduced with pHIV-Luc-ZsGreen lentivirus and

773 sorted on a FACS Aria flow cytometer (BD) for GFP expression. 3 x $10^4$ target cells were
774 seeded in wells of a 96-well round bottom plate. CAR T cells from one of three healthy
775 donors were cocultured with target cells at the indicated effector-target ratios and
776 incubated for 16 hours at 37˚C, 5% $CO_2$. Following incubation, 80 µL of supernatant was
777 harvested from each well. Cells were suspended by gentle pipetting, and 100 µL was
778 transferred to a 96-well black flat bottom plate. D-Luciferin (Gold Biotechnology, catalog
779 no. LUCNA-2G) at 150 µg/mL was added to the cells and incubated for 5 minutes at 37°C.
780 Luminescence was determined on a Spark multimode plate reader (Tecan).

781 **Serial coculture repeat stimulation assay**

782 To determine the long-term *in vitro* control and exhaustion of CAR T cells, luciferase-
783 expressing tumor cells were plated at 5 x $10^4$ cells/well. CAR T cells were cocultured at a
784 defined effector-target ratio and incubated for 24-48 hours at 37˚C, 5% $CO_2$. Following
785 incubation, cells were transferred to a 96-well black flat bottom plate. D-luciferin was
786 added to cells and luminescence was determined on a Spark multimode plate reader
787 (Tecan). After measuring luminescence, cells were washed with FACS buffer and stained
788 with Zombie NIR fixable viability dye (Biolegend) and antibodies targeting CD19, HA, PD-
789 1, TIM-3, CD45RA, and CD62L. Accucheck counting beads (Life Technologies) were
790 added to the cells for normalization. Next, remaining CAR cells were pooled together and
791 normalized based on expansion. CAR T cells were redistributed to wells and fresh tumor
792 cells were added to each well. Plates were incubated for 48 hours at 37˚C, 5% $CO_2$.
793 Luminescence measurements and normalization were repeated until a loss of cytotoxicity
794 was observed.

795 **Cystatin A enzyme-linked immunosorbent assay**

796 Cystatin A concentration was assessed using a Human Cystatin A ELISA kit (Invitrogen,
797 catalog no. EH140RB). Total cell lysates were extracted from CAR T cells using
798 radioimmunoprecipitation assay (RIPA) buffer (Thermo) containing protease inhibitor
799 cocktail (Roche). Total protein concentration was determined using Pierce BCA assay
800 (Thermo). Cystatin A levels were determined by enzyme-linked immunosorbent assay
801 (ELISA) according to manufacturer's instructions (Invitrogen) and calculated using
802 standard curve interpolation. Absorbance was measured at the recommended
803 wavelength on a Spark multimode plate reader (Tecan).

804 **Cathepsin B activity assay**

805 Cathepsin B activity was assessed using the InnoZyme Cathepsin B Activity Assay Kit
806 (MilliPore Sigma, catalog no. CBA001). Total cell lysates were extracted from CAR T cells
807 using the provided cell lysis buffer according to manufacturer's instructions. Total protein
808 concentration was determined using Pierce BCA assay (Thermo Fisher Scientific).
809 Cathepsin B activity was determined fluorometrically according to manufacturer's
810 instructions (Calbiochem). Fluorescence was measured on a Spark multimode plate
811 reader (Tecan).

812 **Treatment of CAR T cells with inhibitors**

813 FMC63 CAR T cells were treated with small-molecule inhibitors targeting Actin (inhibitor:
814 Cytochalasin D, Sigma Aldrich catalog no. C8273), Dynamin (inhibitor: DynaSore, Sigma
815 Aldrich catalog no. D7693), Cathepsin B (inhibitor: Ca-074-Me, SelleckChem catalog no.
816 S7420), Clathrin (inhibitor: PitStop, Abcam catalog no. ab120687), or LFA-1 (inhibitor: BI-

817 1950, Boehringer Ingelheim) at the indicated concentrations for one hour. Following
818 treatment, cells were washed with T cell media and centrifuged at 400 x g for 5 minutes.
819 To determine the effect of the non-membrane permeable CTSB inhibitor CA-074
820 (Millipore Sigma, catalog no. 205530), the inhibitor was added directly to the co-culture
821 at the indicated concentrations. As a control, CAR T cells treated with DMSO. CAR T cells
822 were cocultured with CD19-expressing tumor cells for the indicated intervals.

823 **Western blot**

824 Total cell lysates were extracted from CAR T cells using radioimmunoprecipitation assay
825 (RIPA) buffer (Thermo Fisher Scientific) containing protease inhibitor (Roche). Total
826 protein concentration was determined using Pierce BCA assay (Thermo Fisher Scientific).
827 Samples were separated by SDS–polyacrylamide gel electrophoresis, and separated
828 proteins were transferred to nitrocellulose membranes using an iBlot2 transfer system
829 (Thermo Fisher Scientific). Membranes were blocked with 5% nonfat milk–tris-buffered
830 saline and incubated with primary antibodies against CD19, mCSTA, CISH, or β-actin.
831 Membranes were washed and developed using species-specific secondary anti-
832 IgG/horseradish peroxidase antibodies (R&D Systems) and Western Lightning Plus-ECL
833 solution (PerkinElmer). Bands were visualized and quantified on an iBright 1500 imaging
834 system (Thermo Fisher Scientific).

835 ***In vivo* cystatin A toxicity**

836 6-8 week-old NOD.*Cg-Rag1*$^{tm1Mom}$*Il2rg*$^{tm1Wjl}$/SzJ (NRG) mice (Jackson Laboratory) were
837 irradiated with a sublethal dose of 200 cGy (Rad-Source 2000) and that same day injected
838 with the indicated number of CAR T cells into the lateral tail vein. To assess toxicity,

839 animals were weighed daily and monitored for signs of distress in accordance with
840 institutional regulations. After 14 days, mice were euthanized and lungs, spleens, liver,
841 and gastrointestinal organs were collected, sectioned, and underwent H&E staining to
842 assess organ structure. Slides were imaged using a BZ-X810 fluorescence microscope
843 (Keyence) and BZ-X800 analyzer.

844 **Secretome analysis**

845 CAR and $CAR_{CSTA}$ secretomes were analyzed by Codeplex assay (IsoPlexis). Following
846 production and cryopreservation, CAR and $CAR_{CSTA}$ T cells produced from three healthy
847 donors were thawed and cultured in T cell media + 40IU IL-2 for 48 hours. Cells were
848 activated using anti-CD3/CD28 activation beads (Thermo Fisher) and incubated for 24
849 hours. Supernatants were collected after 24 hours, and cytokine profiling was measured
850 using IsoPlexis Codeplex (Kcas Bio).

851 **Bulk RNA sequencing**

852 Following production and cryopreservation, CAR and $CAR_{CSTA}$ T cells from two
853 independent productions were thawed and cultured in T cell media + 40IU IL-2 for 48
854 hours. After 48 hours, CAR T cells were washed with FACS buffer, stained with anti-CD3,
855 anti-HA, and DAPI, and sorted for CAR expression. Sorted CAR T cells were then pelleted
856 and flash frozen. RNA was extracted, polyA-enriched, and sequenced using Illumina
857 NovaSeq S4 PE100 sequencing targeting 10 million read pairs per sample.

858 ***In vivo* cystatin A model of CAR T cell tumor control and persistence**

859 6–8-week-old male NOD.*Cg-Rag1*$^{tm1Mom}$*Il2rg*$^{tm1Wjl}$/SzJ (NRG) mice (Jackson Laboratory)
860 were irradiated with a sublethal dose of 200 cGy (Day 0). That same day, mice were

861 injected with 4 x $10^5$ NALM6 tumor cells via tail vein injection. On Day 4, mice were
862 injected with 1 x $10^6$ FMC63 CAR or $CAR_{CSTA}$ T cells or CAR T cells lacking a binding
863 domain (ΔscFv) via tail vein injection. Animals were weighed twice weekly and monitored
864 for signs of distress in accordance with institutional regulations. Tumor burden was
865 assessed weekly in prone and supine position by an *in vivo* imaging system (IVIS). For *in*
866 *vivo* imaging, mice received an intraperitoneal injection of 3.3 mg D-luciferin (GOLDBIO
867 # LUCK-10G). On day 28, animals were euthanized and tissues collected for analysis by
868 flow cytometry. Average radiance values (p/s/$cm^2$/sr) were determined using Living
869 Image 4.8 software (PerkinElmer).

870 ***In vivo* model of CAR T cell solid tumor infiltration**

871 6-8 week-old NOD.*Cg-Rag1*$^{tm1Mom}$*Il2rg*$^{tm1Wjl}$/SzJ (NRG) mice (Jackson Laboratory) were
872 irradiated with a sublethal dose of 200 cGy (Rad-Source 2000) and that same day injected
873 intratibially with the indicated number of luciferase-expressing A673 cells (A673-Fluc)
874 expressing CD19-GFP. On Day 14 after tumor cell injection, the indicated number of
875 ΔscFv, FMC63 $CISH^{WT}$ CAR, or $CISH^{KO}$ $CAR_{CSTA}$ T cells were injected into the lateral tail
876 vein. 4 days after CAR T cell injection, mice were euthanized and tumors were collected
877 and dissociated using the Human Tumor Dissociation Kit (Miltenyi Biotec, cat # 130-095-
878 929) and the OctoMACS tissue dissociator (Miltenyi Biotec). CAR T cells were quantified
879 and phenotyped by flow cytometry.

880 ***In vivo* model of CAR T cell solid tumor control**

881 6-8 week-old NOD.*Cg-Rag1*$^{tm1Mom}$*Il2rg*$^{tm1Wjl}$/SzJ (NRG) mice (Jackson Laboratory) were
882 irradiated with a sublethal dose of 200 cGy (Rad-Source 2000) and that same day injected

883 intratibially with the indicated number of luciferase-expressing A673 cells (A673-Fluc)
884 expressing CD19-GFP. On Day 7 after tumor cell injection, the indicated number of
885 ΔscFv, FMC63 $CISH^{WT}$ CAR, or $CISH^{KO}$ $CAR_{CSTA}$ T cells were injected into the lateral tail
886 vein. Tumor burden was assessed weekly by *in vivo* imaging system (IVIS). For *in vivo*
887 imaging, mice received an intraperitoneal injection of 3.3 mg D-luciferin (GOLDBIO #
888 LUCK-10G). Peripheral blood was collected on Day 19 after CAR T cell injection for CAR
889 T cell quantification and phenotyping by flow cytometry.

890 **Statistical Analysis**

891 The respective statistical tests are stated in the figure legends. Generally, statistical
892 significance between two groups was determined by two-sided Student's *t*-test or Mann-
893 Whitney U test. Statistical significance between groups of three or more was determined
894 by one- or two-way analysis of variance (ANOVA). All statistical tests were performed
895 using Prism 10 (GraphPad). Results were considered significant when $p < 0.05$. * = $p <$
896 $0.05$; ** = $p < 0.01$; *** = $p < 0.001$; **** = $p < 0.0001$.
897

898 **Acknowledgements**

899 The authors thank the Flow Cytometry Shared Service of the University of Maryland
900 Marlene and Stewart Greenebaum Comprehensive Cancer Center for help with sorting
901 cells and panel design. We thank Dr. Nevil Singh at the University of Maryland, Baltimore
902 for use of the Keyence BZ-X810 fluorescence microscope. RNA sequencing and the
903 associated analysis was performed by Maryland Genomics at the Institute for Genome
904 Sciences, University of Maryland School of Medicine. Research reported in this
905 publication utilized the Preclinical Research Shared Resource at Huntsman Cancer
906 Institute at the University of Utah and was supported by the National Cancer Institute of
907 the National Institutes of Health under Award Number P30CA042014. This work was
908 supported by funds through the Maryland Department of Health's Cigarette Restitution
909 Fund Program (CH-649-CRF), the National Cancer Institute Cancer Center Support Grant
910 (P30CA134274), the National Institutes of Health to AU (R35 GM145313), and by an
911 NIAID-funded predoctoral fellowship to JMB (T32 AI095190). The plasmid pHIV-Luc-
912 ZsGreen was a gift from Dr. B. Welm (Addgene #39196). The plasmid
913 SFG.CNb30_opt.IRES.eGFP was a gift from Dr. M. Pule (Addgene #22493). The content
914 is solely the responsibility of the authors and does not necessarily represent the official
915 views of the NIH.

916 **Author contributions**

917 KAD and TL conceived the project, planned and performed experiments, analyzed data,
918 and wrote the manuscript. KAD performed the majority of the described *in vitro*
919 experiments, generated the majority of transgenic T cells, developed the CompLuc assay,

920 identified and validated the role of CTSB in CMT, and developed the CSTA-based
921 approach of CMT inhibition in CAR T cells. KN and AP performed confocal microscopy
922 and fixed coculture staining and imaging. FF wrote analysis scripts for CTSB dispersion.
923 MGF and SVR generated FOLRα CAR T cells. JMB planned experiments, analyzed data,
924 and edited the manuscript. EG performed CAR T cell phenotyping and analyzed data.
925 WS, ER, and DL planned and performed *in vivo* models and analyzed data. DY, RM, and
926 AW planned experiments and analyzed data. XF developed full-spectrum flow cytometry
927 panel and performed flow cytometry analysis. DA supervised CAR T cell phenotyping. AU
928 planned and supervised microscopy experiments and analyzed data. TL supervised all
929 work related to this project. All authors reviewed and approved the manuscript.

930 **Competing interests**

931 KAD and TL are inventors on patent application number PCT/US24/53867 describing
932 therapeutic targeting of tumor escape by CAR-mediated trogocytosis. TL receives a
933 salary from AbbVie.

934 **REFERENCES**


935 1. Sadelain, M. CD19 CAR T Cells. *Cell* **171**, 1471 (2017).
936 2. Maude, S. L. *et al.* Tisagenlecleucel in Children and Young Adults with B-Cell Lymphoblastic
937 Leukemia. *N. Engl. J. Med.* **378**, 439–448 (2018).
938 3. Sadelain, M., Rivière, I. & Riddell, S. Therapeutic T cell engineering. *Nature* **545**, 423–431
939 (2017).
940 4. Raje, N. *et al.* Anti-BCMA CAR T-Cell Therapy bb2121 in Relapsed or Refractory Multiple
941 Myeloma. *N. Engl. J. Med.* **380**, 1726–1737 (2019).
942 5. D'Agostino, M. & Raje, N. Anti-BCMA CAR T-cell therapy in multiple myeloma: can we do
943 better? *Leukemia* **34**, 21–34 (2020).
944 6. Romanski, A. *et al.* CD19-CAR engineered NK-92 cells are sufficient to overcome NK cell
945 resistance in B-cell malignancies. *J. Cell. Mol. Med.* **20**, 1287–1294 (2016).
946 7. Boissel, L. *et al.* Retargeting NK-92 cells by means of CD19- and CD20-specific chimeric
947 antigen receptors compares favorably with antibody-dependent cellular cytotoxicity.
948 *OncoImmunology* **2**, e26527 (2013).
949 8. Cappell, K. M. & Kochenderfer, J. N. Long-term outcomes following CAR T cell therapy:
950 what we know so far. *Nat. Rev. Clin. Oncol.* **20**, 359–371 (2023).
951 9. Lee, A. Obecabtagene Autoleucel: First Approval. *Mol. Diagn. Ther.* 1–5 (2025)
952 doi:10.1007/s40291-025-00771-z.
953 10. Purdum, A., Tieu, R., Reddy, S. R. & Broder, M. S. Direct Costs Associated with Relapsed
954 Diffuse Large B-Cell Lymphoma Therapies. *The Oncologist* **24**, 1229–1236 (2019).
955 11. Kanas, G. *et al.* Epidemiology of diffuse large B-cell lymphoma (DLBCL) and follicular
956 lymphoma (FL) in the United States and Western Europe: population-level projections for
957 2020–2025. *Leukemia & Lymphoma* **63**, 54–63 (2022).
958 12. Grover, P. *et al.* Chimeric antigen receptor T-cell therapy in adults with B-cell acute
959 lymphoblastic leukemia. *Blood Adv* **6**, 1608–1618 (2022).
960 13. Bethge, W. A. *et al.* GLA/DRST real-world outcome analysis of CAR T-cell therapies for
961 large B-cell lymphoma in Germany. *Blood* **140**, 349–358 (2022).
962 14. Pan, J. *et al.* Frequent occurrence of CD19-negative relapse after CD19 CAR T and
963 consolidation therapy in 14 TP53-mutated r/r B-ALL children. *Leukemia* **34**, 3382–3387
964 (2020).
965 15. Wudhikarn, K. *et al.* Interventions and outcomes of adult patients with B-ALL progressing
966 after CD19 chimeric antigen receptor T-cell therapy. *Blood* **138**, 531–543 (2021).
967 16. Finney, O. C. *et al.* CD19 CAR T cell product and disease attributes predict leukemia
968 remission durability. *J. Clin. Investig.* **129**, 2123–2132 (2019).
969 17. Feucht, J. *et al.* Calibration of CAR activation potential directs alternative T cell fates and
970 therapeutic potency. *Nat. Med.* **25**, 82–88 (2019).
971 18. L., M. S. *et al.* Chimeric Antigen Receptor T Cells for Sustained Remissions in Leukemia. *N.*
972 *Engl. J. Med.* **371**, 1507–1517 (2014).
973 19. Zhao, Z. *et al.* Structural Design of Engineered Costimulation Determines Tumor Rejection
974 Kinetics and Persistence of CAR T Cells. *Cancer Cell* **28**, 415–428 (2015).
975 20. Shah, N. N. & Fry, T. J. Mechanisms of resistance to CAR T cell therapy. *Nat Rev Clin*
976 *Oncol* **16**, 372–385 (2019).
977 21. Gardner, R. A. *et al.* Intent-to-treat leukemia remission by CD19 CAR T cells of defined
978 formulation and dose in children and young adults. *Blood* **129**, 3322–3331 (2017).
979 22. Hamieh, M. *et al.* CAR T cell trogocytosis and cooperative killing regulate tumour antigen
980 escape. *Nature* **568**, 112–116 (2019).

981 23. Olson, M. L. *et al.* Low-affinity CAR T cells exhibit reduced trogocytosis, preventing rapid
982 antigen loss, and increasing CAR T cell expansion. *Leukemia* **36**, 1943–1946 (2022).
983 24. Li, Y. *et al.* KIR-based inhibitory CARs overcome CAR-NK cell trogocytosis-mediated
984 fratricide and tumor escape. *Nat Med* **28**, 2133–2144 (2022).
985 25. Ahmed, K. A., Munegowda, M. A., Xie, Y. & Xiang, J. Intercellular Trogocytosis Plays an
986 Important Role in Modulation of Immune Responses. *Cell. Mol. Immunol.* **5**, 261–269
987 (2008).
988 26. Huang, J.-F. *et al.* TCR-Mediated Internalization of Peptide-MHC Complexes Acquired by T
989 Cells. *Science* **286**, 952–954 (1999).
990 27. Mause, E. R. V. *et al.* Systematic single amino acid affinity tuning of CD229 CAR T cells
991 retains efficacy against multiple myeloma and eliminates on-target off-tumor toxicity. *Sci.*
992 *Transl. Med.* **15**, eadd7900 (2023).
993 28. Camviel, N. *et al.* Both APRIL and antibody-fragment-based CAR T cells for myeloma
994 induce BCMA downmodulation by trogocytosis and internalization. *J. Immunother. Cancer*
995 **10**, e005091 (2022).
996 29. Cohen, A. D. *et al.* B cell maturation antigen-specific CAR T cells are clinically active in
997 multiple myeloma. *J. Clin. Investig.* **129**, 2210–2221 (2019).
998 30. Radhakrishnan, S. V. *et al.* CD229 CAR T cells eliminate multiple myeloma and tumor
999 propagating cells without fratricide. *Nat. Commun.* **11**, 798 (2020).
1000 31. Bu, D.-X. *et al.* Pre-clinical validation of B cell maturation antigen (BCMA) as a target for T
1001 cell immunotherapy of multiple myeloma. *Oncotarget* **9**, 25764–25780 (2018).
1002 32. Marei, H. *et al.* Antibody targeting of E3 ubiquitin ligases for receptor degradation. *Nature*
1003 **610**, 182–189 (2022).
1004 33. Békés, M., Langley, D. R. & Crews, C. M. PROTAC targeted protein degraders: the past is
1005 prologue. *Nat. Rev. Drug Discov.* **21**, 181–200 (2022).
1006 34. Billerhart, M. *et al.* Recombinant Human CD19 in CHO-K1 Cells: Glycosylation Patterns as
1007 a Quality Attribute of High Yield Processes. *Int. J. Mol. Sci.* **24**, 10891 (2023).
1008 35. Heard, A. *et al.* Antigen glycosylation regulates efficacy of CAR T cells targeting CD19. *Nat.*
1009 *Commun.* **13**, 3367 (2022).
1010 36. Brooks, S. R., Kirkham, P. M., Freeberg, L. & Carter, R. H. Binding of Cytoplasmic Proteins
1011 to the CD19 Intracellular Domain Is High Affinity, Competitive, and Multimeric. *J. Immunol.*
1012 **172**, 7556–7564 (2004).
1013 37. Ruella, M. *et al.* Induction of resistance to chimeric antigen receptor T cell therapy by
1014 transduction of a single leukemic B cell. *Nat. Med.* **24**, 1499–1503 (2018).
1015 38. Dixon, A. S. *et al.* NanoLuc Complementation Reporter Optimized for Accurate
1016 Measurement of Protein Interactions in Cells. *ACS Chem. Biol.* **11**, 400–408 (2016).
1017 39. Miyake, K. *et al.* Trogocytosis of peptide-MHC class II complexes from dendritic cells
1018 confers antigen-presenting ability on basophils. *Proc Natl Acad Sci U S A* **114**, 1111–1116
1019 (2017).
1020 40. Gilmartin, A. A., Ralston, K. S. & Petri, W. A. Inhibition of Amebic Cysteine Proteases
1021 Blocks Amebic Trogocytosis but Not Phagocytosis. *J. Infect. Dis.* **221**, 1734–1739 (2020).
1022 41. Reed, J., Reichelt, M. & Wetzel, S. A. Lymphocytes and Trogocytosis-Mediated Signaling.
1023 *Cells* **10**, 1478 (2021).
1024 42. Hudrisier, D., Aucher, A., Puaux, A.-L., Bordier, C. & Joly, E. Capture of Target Cell
1025 Membrane Components via Trogocytosis Is Triggered by a Selected Set of Surface
1026 Molecules on T or B Cells. *J. Immunol.* **178**, 3637–3647 (2007).
1027 43. Cavallo-Medved, D., Moin, K. & Sloane, B. Cathepsin B. *AFCS Nat Mol Pages* **2011**,
1028 A000508 (2011).

1029 44. Mort, J. S. & Buttle, D. J. Cathepsin B. *Int. J. Biochem. Cell Biol.* **29**, 715–720 (1997).
1030 45. Vidak, E., Javoršek, U., Vizovišek, M. & Turk, B. Cysteine Cathepsins and Their Extracellular
1031 Roles: Shaping the Microenvironment. *Cells* **8**, 264 (2019).
1032 46. Balaji, K. N., Schaschke, N., Machleidt, W., Catalfamo, M. & Henkart, P. A. Surface
1033 Cathepsin B Protects Cytotoxic Lymphocytes from Self-destruction after Degranulation.
1034 *Journal of Experimental Medicine* **196**, 493–503 (2002).
1035 47. Olson, O. C. & Joyce, J. A. Cysteine cathepsin proteases: regulators of cancer progression
1036 and therapeutic response. *Nat Rev Cancer* **15**, 712–729 (2015).
1037 48. Gabrijelcic, D. *et al.* Cathepsins B, H and L in human breast carcinoma. *Eur J Clin Chem*
1038 *Clin Biochem* **30**, 69–74 (1992).
1039 49. Estrada, S. *et al.* The Role of Gly-4 of Human Cystatin A (Stefin A) in the Binding of Target
1040 Proteinases. Characterization by Kinetic and Equilibrium Methods of the Interactions of
1041 Cystatin A Gly-4 Mutants with Papain, Cathepsin B, and Cathepsin L. *Biochemistry* **37**,
1042 7551–7560 (1998).
1043 50. Pavlova, A., Krupa, J. C., Mort, J. S., Abrahamson, M. & Björk, I. Cystatin inhibition of
1044 cathepsin B requires dislocation of the proteinase occluding loop. Demonstration by
1045 release of loop anchoring through mutation of His110. *FEBS Lett.* **487**, 156–160 (2000).
1046 51. Pavlova, A. & Björk, I. Grafting of Features of Cystatins C or B into the N-Terminal Region
1047 or Second Binding Loop of Cystatin A (Stefin A) Substantially Enhances Inhibition of
1048 Cysteine Proteinases. *Biochemistry* **42**, 11326–11333 (2003).
1049 52. Guicciardi, M. E., Miyoshi, H., Bronk, S. F. & Gores, G. J. Cathepsin B Knockout Mice Are
1050 Resistant to Tumor Necrosis Factor-α-Mediated Hepatocyte Apoptosis and Liver Injury
1051 Implications for Therapeutic Applications. *Am. J. Pathol.* **159**, 2045–2054 (2001).
1052 53. Vasiljeva, O. *et al.* Reduced tumour cell proliferation and delayed development of high-
1053 grade mammary carcinomas in cathepsin B-deficient mice. *Oncogene* **27**, 4191–4199
1054 (2008).
1055 54. Hook, G. *et al.* Cathepsin B Gene Knockout Improves Behavioral Deficits and Reduces
1056 Pathology in Models of Neurologic Disorders. *Pharmacol. Rev.* **74**, 600–629 (2022).
1057 55. Deussing, J. *et al.* Cathepsins B and D are dispensable for major histocompatibility
1058 complex class II-mediated antigen presentation. *Proc. Natl. Acad. Sci.* **95**, 4516–4521
1059 (1998).
1060 56. Jenko, S. *et al.* Different propensity to form amyloid fibrils by two homologous proteins—
1061 Human stefins A and B: Searching for an explanation. *Proteins: Struct., Funct., Bioinform.*
1062 **55**, 417–425 (2004).
1063 57. Xu, X. *et al.* Mechanisms of Relapse After CD19 CAR T-Cell Therapy for Acute
1064 Lymphoblastic Leukemia and Its Prevention and Treatment Strategies. *Front. Immunol.* **10**,
1065 2664 (2019).
1066 58. Gu, T., Zhu, M., Huang, H. & Hu, Y. Relapse after CAR-T cell therapy in B-cell
1067 malignancies: challenges and future approaches. *J. Zhejiang Univ.-Sci. B* **23**, 793–811
1068 (2022).
1069 59. Lu, Z. *et al.* ATF3 and CH25H regulate effector trogocytosis and anti-tumor activities of
1070 endogenous and immunotherapeutic cytotoxic T lymphocytes. *Cell Metab.* **34**, 1342-
1071 1358.e7 (2022).
1072 60. Barbera, S. *et al.* Trogocytosis of chimeric antigen receptors between T cells is regulated
1073 by their transmembrane domains. *Sci. Immunol.* **10**, eado2054 (2025).
1074 61. Ruella, M. *et al.* Induction of resistance to chimeric antigen receptor T cell therapy by
1075 transduction of a single leukemic B cell. *Nat. Med.* **24**, 1499–1503 (2018).

1076 62. Jin, L. L. *et al.* Tyrosine Phosphorylation of the Lyn Src Homology 2 (SH2) Domain
1077 Modulates Its Binding Affinity and Specificity*[S]. *Mol. Cell. Proteom.* **14**, 695–706 (2015).
1078 63. Stover, D. R., Furet, P. & Lydon, N. B. Modulation of the SH2 Binding Specificity and
1079 Kinase Activity of Src by Tyrosine Phosphorylation within Its SH2 Domain (∗). *J. Biol. Chem.*
1080 **271**, 12481–12487 (1996).
1081 64. Xu, Y., Harder, K. W., Huntington, N. D., Hibbs, M. L. & Tarlinton, D. M. Lyn Tyrosine Kinase
1082 Accentuating the Positive and the Negative. *Immunity* **22**, 9–18 (2005).
1083 65. Towatari, T. *et al.* Novel epoxysuccinyl peptides A selective inhibitor of cathepsin B, in vivo.
1084 *FEBS Lett.* **280**, 311–315 (1991).
1085 66. Murata, M. *et al.* Novel epoxysuccinyl peptides Selective inhibitors of cathepsin B, in vitro.
1086 *FEBS Lett.* **280**, 307–310 (1991).
1087 67. Turk, V. & Bode, W. The cystatins: Protein inhibitors of cysteine proteinases. *FEBS Lett.*
1088 **285**, 213–219 (1991).
1089 68. Smole, A. *et al.* Expression of inducible factors reprograms CAR-T cells for enhanced
1090 function and safety. *Cancer Cell* **40**, 1470-1487.e7 (2022).
1091 69. Allen, G. M. *et al.* Synthetic cytokine circuits that drive T cells into immune-excluded
1092 tumors. *Science* **378**, eaba1624–eaba1624 (2022).
1093 70. Prunk, M. *et al.* Extracellular Cystatin F Is Internalised by Cytotoxic T Lymphocytes and
1094 Decreases Their Cytotoxicity. *Cancers* **12**, 3660 (2020).
1095 71. Magister, Š., Tseng, H.-C., Bui, V. T., Kos, J. & Jewett, A. Regulation of split anergy in
1096 natural killer cells by inhibition of cathepsins C and H and cystatin F. *Oncotarget* **6**, 22310–
1097 22327 (2015).
1098 72. Lu, Z. *et al.* ATF3 and CH25H regulate effector trogocytosis and anti-tumor activities of
1099 endogenous and immunotherapeutic cytotoxic T lymphocytes. *Cell Metab.* **34**, 1342-
1100 1358.e7 (2022).
1101 73. Palmer, D. C. *et al.* Cish actively silences TCR signaling in CD8+ T cells to maintain tumor
1102 tolerance. *J. Exp. Med.* **212**, 2095–2113 (2015).
1103 74. Lv, J. *et al.* Disruption of CISH promotes the antitumor activity of human T cells and
1104 decreases PD-1 expression levels. *Mol. Ther. - Oncolytics* **28**, 46–58 (2023).
1105 75. Lv, J. *et al.* Disruption of CISH promotes the antitumor activity of human T cells and
1106 decreases PD-1 expression levels. *Mol. Ther. - Oncolytics* **28**, 46–58 (2023).
1107 76. Palmer, D. C. *et al.* Internal checkpoint regulates T cell neoantigen reactivity and
1108 susceptibility to PD1 blockade. *Med* **3**, 682-704.e8 (2022).
1109 77. Newick, K., O'Brien, S., Moon, E. & Albelda, S. M. CAR T Cell Therapy for Solid Tumors.
1110 *Annu. Rev. Med.* **68**, 139–152 (2016).
1111 78. Sterner, R. C. & Sterner, R. M. CAR-T cell therapy: current limitations and potential
1112 strategies. *Blood Cancer J.* **11**, 1–11 (2021).
1113 79. Lee, D. W. *et al.* T cells expressing CD19 chimeric antigen receptors for acute
1114 lymphoblastic leukaemia in children and young adults: a phase 1 dose-escalation trial.
1115 *Lancet* **385**, 517–528 (2015).
1116 80. Veatch, S. L. *et al.* Correlation Functions Quantify Super-Resolution Images and Estimate
1117 Apparent Clustering Due to Over-Counting. *PLoS ONE* **7**, e31457 (2012).
1118